CIVIL ENGINEERING STUDIES
Illinois Center for Transportation Series No. 24-025
UILU-ENG-2024-2025
ISSN: 0197-9191

Load Rating of Reinforced Concrete Slab Bridges Using Field Testing

Prepared By
Bassem Andrawes
Isaias Andres Colombani
Md Abdul Hamid Mirdad
Alexander Jai-syn Chen
University of Illinois Urbana-Champaign

Research Report No. FHWA-ICT-24-022

A report of the findings of

ICT PROJECT R27-205
Development of Bridge Load Testing Program for Load Rating of Concrete Bridges

https://doi.org/10.36501/0197-9191/24-025

Illinois Center for Transportation

December 2024

TECHNICAL REPORT DOCUMENTATION PAGE

1. Report No.	2. Government Accession No.	3. Recipient's Catalog No.
FHWA-ICT-24-022	N/A	N/A

4. Title and Subtitle	5. Report Date
Load Rating of Reinforced Concrete Slab Bridges Using Field Testing	December 2024
	6. Performing Organization Code N/A

7. Authors	8. Performing Organization Report No.
Bassem Andrawes (https://orcid.org/0000-0002-8954-3751), Isaias A. Colombani, Md Abdul H. Mirdad (https://orcid.org/0000-0002-0114-5979), Alexander J. Chen (https://orcid.org/0009-0002-0657-4323)	ICT-24-025 UILU-2024-2025

9. Performing Organization Name and Address	10. Work Unit No.
Illinois Center for Transportation Department of Civil and Environmental Engineering University of Illinois Urbana-Champaign 205 North Mathews Avenue, MC-250 Urbana, IL 61801	N/A **11. Contract or Grant No.** R27-205

12. Sponsoring Agency Name and Address	13. Type of Report and Period Covered
Illinois Department of Transportation (SPR) Bureau of Research 126 East Ash Street Springfield, IL 62704	Final Report 7/16/19–12/15/24 **14. Sponsoring Agency Code**

15. Supplementary Notes

Conducted in cooperation with the U.S. Department of Transportation, Federal Highway Administration.
https://doi.org/10.36501/0197-9191/24-025

16. Abstract

Bridge load-rating analysis is typically used to assess the safe load-carrying capacity of bridges. However, in many cases, this analytical approach was proven to be too conservative, which leads to unnecessary bridge postings and road restrictions. In such cases, field testing is sought as a more reliable method for assessing the structural condition of the investigated bridge. This study focused on investigating the efficacy and practicality of performing load rating on reinforced concrete slab bridges in Illinois using two field testing methods—namely, diagnostic and proof load testing. The versatility of both methods was examined through testing six different slab bridges of varying characteristics and conditions. The tested bridges included single- and double-span bridges with span lengths varying between 20.5 ft and 32 ft, and skew angles varying between 0 and 55 degrees. The bridges also varied in age, with the first tested bridge's construction dating as far back as 1925. The research assessed the type of instrumentation and data acquisition system used as well as the challenges associated with setting up these devices in the field. The analytical and field-based load-rating factors were compared for each bridge. The results showed the effectiveness of field testing in providing a relatively fast and reliable assessment of the structural condition of the investigated bridges. The methods adopted and developed in this research will assist the Illinois Department of Transportation in making future decisions about the condition of bridges in Illinois.

17. Key Words	18. Distribution Statement
AASHTO, Load Rating, LFR, MBE, Effective Width, Diagnostic Test, Proof Load Test, Reinforced Concrete Bridge, Slab Bridges	No restrictions. This document is available through the National Technical Information Service, Springfield, VA 22161.

19. Security Classif. (of this report)	20. Security Classif. (of this page)	21. No. of Pages	22. Price
Unclassified	Unclassified	73	N/A

ACKNOWLEDGMENT, DISCLAIMER, MANUFACTURERS' NAMES

This publication is based on the results of **ICT-R27-205: Development of Bridge Load Testing Program for Load Rating of Concrete Bridges**. ICT-R27-205 was conducted in cooperation with the Illinois Center for Transportation; the Illinois Department of Transportation; and the U.S. Department of Transportation, Federal Highway Administration.

Members of the Technical Review Panel (TRP) were the following:

- Ruben Boehler, TRP Chair, Illinois Department of Transportation
- William Beisner, Illinois Department of Transportation
- Steve Beran, Illinois Department of Transportation
- Dan Colwell, Richland County
- Keith Donovan, Illinois Department of Transportation
- Chris Hahin, Illinois Department of Transportation
- Spencer Koehler, Illinois Department of Transportation
- Nick Lombardi, Federal Highway Administration
- Robert Perkins, Illinois Department of Transportation
- Frank Sharpe, Federal Highway Administration
- Dan Zerrusen, Illinois Department of Transportation

EXECUTIVE SUMMARY

Bridge load-rating analysis has been used for decades to assess the safe load-carrying capacity of bridges in the United States. As time progressed, bridges that were rated using American Association of State Highway and Transportation Officials (AASHTO) analytical load-rating methods began to show lower load capacities than those that the bridges have proven to carry through load-testing alternatives. This is especially true for reinforced concrete (RC) slab bridges, which have complicated load path distributions and often benefit from load tests. This has resulted in unnecessary roadway restrictions, bridge closures, and other inconveniences to the communities that rely on these bridges for daily commutes.

This study investigated the efficacy and practicality of performing load rating on RC slab bridges in Illinois using two field testing methods—namely, diagnostic and proof load testing. The versatility of both methods was examined through testing six different slab bridges of varying characteristics and conditions. Different approaches were adopted and compared for calculating the load-rating factors of the investigated bridges. The first is the AASHTO Load Factor Rating (LFR) procedure, which does not require testing of the bridge. The second is the AASHTO Manual for Bridge Evaluation (MBE) approach, which was used for both diagnostic and proof load tests. The ratings were also modified using an effective strip width (EW) procedure.

Field tests were conducted using Bridge Diagnostics Inc.'s fourth-generation structural testing system, STS4. The system was compatible with linear variable differential transformers, strain gauges, and tiltmeters. The information was transferred from sensors to nodes, then to a wireless base station, and then into a laptop. The type of sensor and amount needed were chosen based on the bridge geometry and site conditions.

Six bridges were chosen for the diagnostic and proof load tests to determine the advantages of load testing over analytical load rating. The bridges were chosen to vary in length and width as well as in skewness. The tested bridges included single- and double-span bridges with span lengths varying between 20.5 ft (6.2 m) and 32 ft (9.8 m), and skew angles varying between 0 and 55 degrees. The bridges also varied in age, with the oldest bridge constructed in 1925. The research assessed the type of instrumentation and data acquisition system used as well as the challenges associated with setting up these devices in the field. The analytical and field-based load-rating factors were compared for each bridge. The results showed the effectiveness of field testing in providing a relatively fast and reliable assessment of the structural condition of the investigated bridges. The methods adopted and developed in this research will assist the Illinois Department of Transportation in making future decisions about the condition of bridges in Illinois.

TABLE OF CONTENTS

LIST OF FIGURES

LIST OF TABLES

CHAPTER 1: INTRODUCTION

PROBLEM DESCRIPTION

Analytical load-rating procedures following the American Association of State Highway and Transportation Officials (AASHTO) *Manual for Bridge Evaluation* (*MBE*) guidelines have been the prominent means for load rating bridges for structural capacity evaluations (AASHTO, 2018). During this process, each bridge is analyzed using one or several hypothetical legal rating vehicles as defined by the *MBE* to determine if the bridge must be load posted to a smaller allowable load capacity and to what extent the bridge must be posted (AASHTO, 2018). These load postings are often encountered on a white roadway sign as drivers approach a bridge. The signs show the maximum tonnage (weight in tons) that vehicles can have to cross the bridge safely. While these load postings are often overlooked by the general public, several larger vehicles used for cargo, agriculture, and other essentials suffer many inconveniences. These consequences have led to problems concerning load-rating analysis procedures. If the analysis is too conservative, then the load postings may unnecessarily restrict the weight of the vehicles that are allowed to use the bridge, impacting the communities that the bridge serves.

In 2022, the Federal Highway Administration (FHWA) reported that 9% of the United States' bridges are classified as poor condition, meaning these bridges may have limits for speed and weight and require significant repair (FHWA, 2022). This amounts to over 46,000 bridges that have load ratings below today's design standards, resulting in load restrictions to numerous busy roadways throughout the United States. Today, many of these bridges are still being evaluated using visual inspection methods and analytical rating procedures following the AASHTO *MBE* guidelines (AASHTO, 2018). These methods have been shown to conservatively underestimate the true capacity for bridges through field testing approaches (Saraf, 1998; Jáuregui et al., 2010; Davids et al., 2013). Consequently, there has been a shift toward load rating using field testing methods for improving the credibility of a bridge's capacity to carry the specified design loads.

Among the commonly used bridge types that have been serving rural and agricultural regions in the U.S. are reinforced concrete (RC) slab bridges. According to FHWA's 2016 National Bridge Inventory data, RC slab bridges account for 10.3% of the U.S. bridge inventory classified to be structurally deficient. Many of these bridges are older RC slab bridges located in rural areas and are often overlooked because of their remote location. Because older bridges have been designed for lesser demands than the currently adopted HL-93 design truck used in the AASHTO specifications (AASHTO, 2020), these bridges are often deemed to be structurally inadequate to carry the design loads imposed today and are posted to smaller load capacities than these bridges have proven to carry through load testing methods (Jorgenson & Larson, 1976; Azizinamini et al., 1994; Miller et al., 1994). Although RC slab bridges are seemingly simple, they have complicated load path distributions that often result in increased load-rating factors (RFs) from those obtained using analytical rating procedures (Commander, 2019). Extensive research has been performed on RC slab bridges to better understand the influence of edge beams, aspect ratio, and skew angle, which were identified to be prominent factors in obtaining more accurate and favorable load ratings for these bridges (Arockiasamy & Amer, 1997, Menassa et al., 2007, Freeman & Vasconcelos, 2018). Because each RC

slab bridge is unique, often having a combination of distinctive skew angles, aspect ratio, and railing conditions, there are still several uncertainties that make these bridges great candidates for load rating using field testing.

SCOPE OF RESEARCH

This research was motivated and supported by the Illinois Department of Transportation (IDOT) to improve load-rating procedures throughout Illinois using load testing and to study the feasibility of using bridge load testing as a load-rating method. To familiarize the reader with the significance of load testing as a viable alternative to the AASHTO *MBE*'s analytical load-rating procedures, diagnostic and proof load field tests were performed on six distinct RC slab bridges that were posted to lesser load capacities using analytical load-rating methods. The analytical load-rating results were compared to the load ratings attained using load testing alternatives to demonstrate the advantages of load testing.

CHAPTER 2: LOAD-RATING PROCEDURES FOR RC SLAB BRIDGES

AASHTO LFR ANALYTICAL RATING PROCEDURE

A rating factor (RF) can be calculated using one-dimensional (1D) beam line analysis and by applying the load factor rating (LFR) equation in Figure 1 provided by the AASHTO *MBE* (AASHTO, 2018):

$$RF = \frac{C - A_1 D}{A_2 L(1 + I)}$$

Figure 1. Equation. Equation for rating factor.

where C is the nominal capacity of the bridge, L and D are the maximum live and dead load effects on the bridge, respectively, I is the impact factor calculated as a function of the span length with a maximum value of 0.3 (AASHTO, 2002), and A_1 and A_2 are the loading factors for operating and inventory level conditions as per the *MBE* (AASHTO, 2018). Because the *MBE* refers to AASHTO standard specifications (2002), these specifications are used for the analytical load rating. The dead load effects are determined by distributing the weight of the curbs and/or railings equally along the width of the slab. The live load effects are obtained by maximizing the effects of the HS-20 design truck wheel loads on a unit-wide strip of the slab. For simple span bridges with reinforcement running parallel to the span, AASHTO provides approximate approaches for calculating the live load effects on the bridge. These approaches include Appendix A in the AASHTO standard specifications (2002) and the following equation (Figure 2) for spans up to and including 15.2 m (50 ft):

$$\mathrm{M}_{LL} = 900\mathrm{S} \ \leq \ 45{,}000$$

Figure 2. Equation. Equation for live load moment.

where M_{LL} is the live load moment in foot-pounds for HS-20 loading, and *S* is the effective span length in feet (AASHTO, 2002). The distribution width equation in Figure 3 was used to determine the effects of the design truck wheel load per unit width:

$$\mathrm{E} = 4 + 0.06\mathrm{S} \ \leq \ 7$$

Figure 3. Equation. Equation for distribution width.

where *E* is the distribution width for a single wheel in feet. The total effective width was calculated by centering the HS-20 design truck(s) on a 3.1 m (10 ft) wide design lane and considering the distribution width for two wheels. The effective width for a single lane load (SLL) is calculated by multiplying the wheel load distribution calculated using Figure 3 by 2, as specified in AASHTO (2002). The wheel spacing used in calculating the effective width for a multilane load (MLL) was 1.2 m (4 ft), representing the spacing of two HS-20 design trucks side-by-side, as presented in Figure 4.

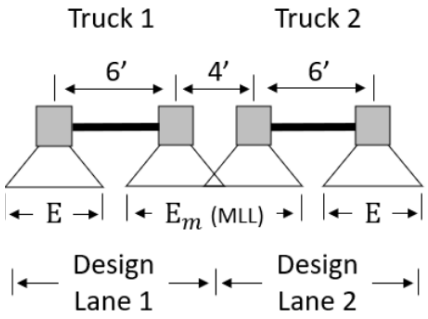

Figure 4. Illustration. Wheel spacing used for effective width calculation of bridge under MLL (E_m).

AASHTO MBE DIAGNOSTIC TESTING PROCEDURE

Diagnostic load testing can be used to determine a modified load rating using the AASHTO MBE approach. The procedure requires that a modified rating factor (RF_T) be calculated using the equation in Figure 5:

$$RF_T = RF_C \times K$$

Figure 5. Equation. Equation for modified rating factor.

where RF_C is the analytical RF and K is an adjustment factor determined from the diagnostic test results in accordance with Figure 6.

$$K = 1 + K_a K_b$$

Figure 6. Equation. Equation for adjustment factor.

In Figure 6, K_a accounts for the benefit or loss derived from the load test and consideration of the section factor resisting the applied load, and K_b accounts for the understanding of the load test results when compared with those predicted by theory (AASHTO, 2018). The *MBE* provides the following general expression to calculate K_a in Figure 7:

$$K_a = \frac{\epsilon_c}{\epsilon_T} - 1$$

Figure 7. Equation. Equation for K_a.

where ϵ_T is the maximum member strain measured during the load test, and ϵ_c is the corresponding calculated strain due to the test vehicle, at its position on the bridge which produced ϵ_T (AASHTO, 2018). Moreover, the *MBE* also provides guidance on selecting the appropriate value for K_b, which utilizes the ratio *T* (the unfactored vehicle effect) by *W* (the unfactored gross rating load effect) to evaluate whether a linear structural response can be extended to amplified load levels. This evaluation is performed to ensure that the structure has enough capacity beyond its rating load level *W*.

AASHTO MBE PROOF LOAD TESTING PROCEDURE

The first step for determining the modified load rating using this approach is to determine the target proof load to achieve an RF of 1.0. This is attained by utilizing a magnification factor (X_p) for establishing a margin of safety due to the current bridge conditions and uncertainties in the test. The *MBE* recommends a value of 1.4 be used as the modification factor with the possibility of adjusting this factor based on the structure type, redundancy, condition, average daily truck traffic (ADTT), and controlling load case (AASHTO, 2018). The new adjusted magnification factor (X_{pA}) is determined as follows in Figure 8:

$$X_{pA} = X_p(1 + \frac{\sum \%}{100})$$

Figure 8. Equation. Equation for X_{pA}.

where ∑% is the summation of the percentage increase and/or reduction recommended by the *MBE* for the above parameters. The target proof load (L_T) can then be determined from the equation in Figure 9:

$$L_T = X_{pA} L_R (1 + I)$$

Figure 9. Equation. Equation for L_T.

where L_R is the comparable unfactored live load due to the rating vehicle for the lanes loaded. After the target load is calculated, the details of the loading steps and procedure must be determined to load the bridge safely. The loads are applied in stages, where each stage is a fraction of L_T applied incrementally and may be loaded and unloaded multiple times to confirm repeatability (AASHTO, 2018). The applied loads and bridge response are monitored carefully during the test to check for any signs of distress in the structure, to which the load testing should be terminated. Once the proof test is completed or terminated, the maximum applied live load (L_p) on the bridge is known and the operating level load rating (RF_o) is determined as follows in Figure 10:

$$RF_o = \frac{\frac{k_0 L_p}{X_{PA}}}{L_R(1 + I)}$$

Figure 10. Equation. Equation for RF_o.

where k_0 is 1.0 when the target proof load is achieved and 0.88 if the test was terminated because of observed distress in the bridge prior to reaching L_T.

STRUCTURAL EFFECTIVE STRIP WIDTH PROCEDURE

The structural effective strip width (EW) approach was another method employed in this study to compute a modified load rating. The basis of this method is to replace the AASHTO LFR EW from the

analytical load-rating analysis with a new measured EW from the test data to solve for a modified RF using Figure 1. The purpose of including this method is to validate whether this approach yields more favorable load ratings than the more conservative AASHTO analytical approach, as verified by several studies (Saraf, 1998; Amer et al., 1999; Jáuregui et al., 2010; Shenton III & Jones, 2012). Also, the EW approach is compared with the AASHTO MBE load rating through load testing approaches discussed previously. In this analysis, the critical moment distribution of the RC slab bridge is used to determine an EW. Edge beams are traditionally considered nonstructural members and were not included in the AASHTO EW calculations (Freeman & Vasconcelos, 2019). Therefore, they have been excluded from this simplified analysis despite demonstrating a favorable influence on the RFs for RC slab bridges in previous studies (Azizinamini et al., 1994; Mabsout et al., 2004). The moments are calculated from the measured strains from the load tests utilizing the elastic stress–strain relation and applying the Euler–Bernoulli theory. An EW is calculated by dividing the area under the curve by the maximum moment observed for the controlling load case. This EW is then used to determine a modified load rating for the bridge.

FIELD TESTING INFORMATION

The instrumentation used to conduct the field tests was the Bridge Diagnostics Inc. (BDI) fourth-generation structural testing system, STS4, presented in Figure 11. The system functions with various components that communicate via a wireless link to transmit data to a computer. The system is built for rugged outdoor use to minimize environmental effects and to prevent damage to the equipment during field tests. The system's main components are the wireless base station (WBS), which provides a wireless interface to the data acquisition system (DAQ) and the computer; the STS4 nodes, which transmit data to the computer and provide power to the connecting sensors; the sensors used for measuring the desired load effects of the bridge; and the computer, which is used to store and visualize the field data. Each component is essential to the operation of the STS4 system and will be discussed in more detail regarding its installation, operation, and limitations.

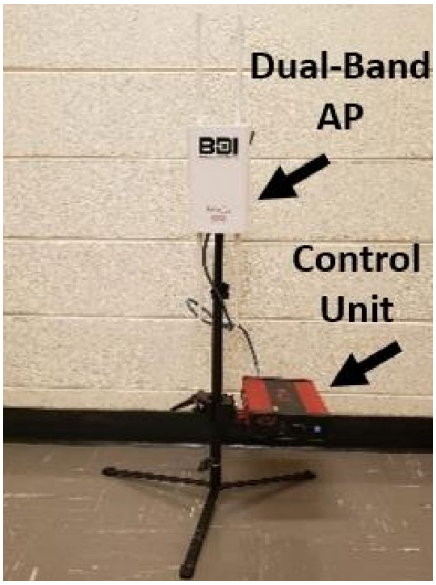

A. WBS

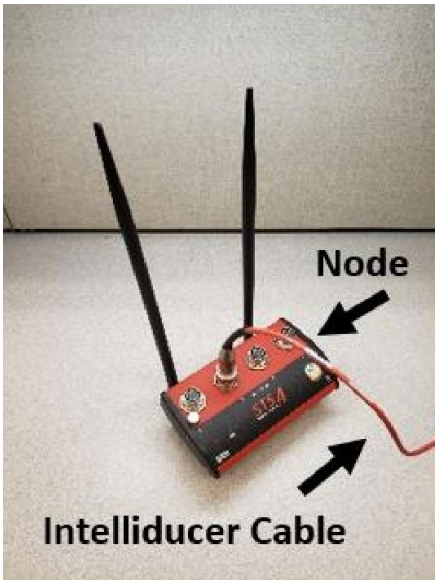

B. Node

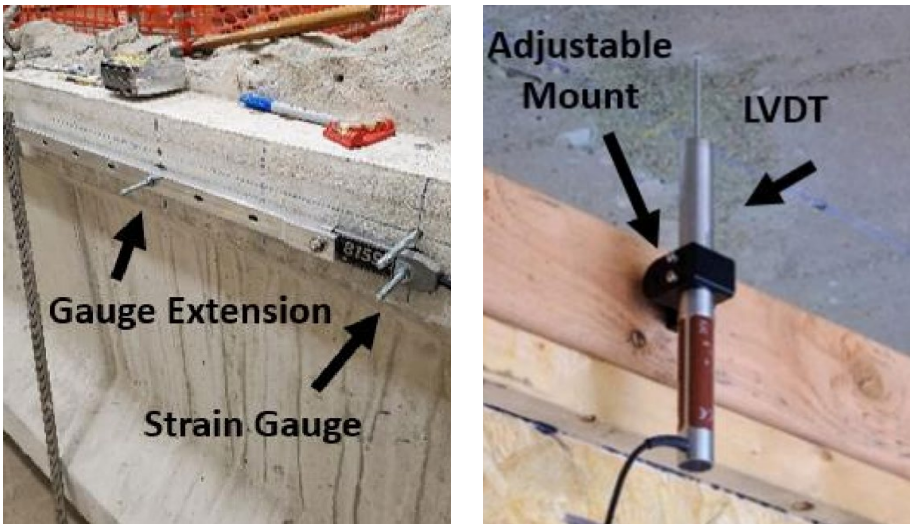

C. ST350 strain gauge D. LVDT

Figure 11. Photo. BDI STS4 instrumentation

As previously mentioned, the WBS provides the wireless access point (AP) for the system. The WBS has a control unit that supplies the dual-band wireless AP with the power needed to function remotely. The control unit has a battery life of approximately 16 hours and is rechargeable. The control unit also functions on an external (wired) 24 VDC power supply in case of long-term monitoring applications. The WBS has ethernet ports for when a wired interface is preferred. In the most ideal conditions, the WBS has a range of 6.4 km (4 mi). However, this range is reliant on the line-of-site and is reduced with physical obstructions between the components. The WBS is mounted on a tripod where the dual-band AP and control unit can be installed for convenient positioning on the field, as presented in Figure 11-A.

The STS4 nodes can accommodate up to four sensors each. A maximum of 128 nodes can be connected using a single WBS for the test. These nodes are equipped with a rechargeable internal battery that can supply power to the sensors for over 40 hours when used at the maximum sampling rate of 1,000 samples per second (S/s). The STS4 nodes have an internal memory of 8 GB for backup data storage. They also have temperature sensor inputs for each channel. The node can operate via a wireless connection to the WBS or ethernet cable. The nodes are lightweight and compact for easy transport during field tests. An image of the STS4 node is presented in Figure 11-B.

Various sensors can be used for bridge monitoring and field-testing applications. However, the most common are linear variable differential transformers (LVDTs) and strain gauges (ST350s) for measuring displacements and strains, respectively. BDI supplies both types of sensors, which are compatible with the STS4 nodes. The LVDTs purchased for the field tests have a range of ±25.4 mm (±1.0 in.) Their total length is 0.3 m (10.8 in.), and they have a supply voltage of 6 to 18 VDC. They were purchased with adjustable aluminum mounting brackets that can be installed on a tripod or other fixture for field tests, as presented in Figure 11-C.

The ST350s are encased in a sealed aluminum shell, making them ideal for outdoor use. They have an effective gauge length of 76.2 mm (3 in.) with the option to add an extension for RC installations up to 0.6 m (24 in.). The ST350s can be installed with the typical adhesive mounting technique by applying the adhesive to the reusable mounting tabs that came with the ST350s. They can also be installed using anchors because they have 6.4 mm (0.25 in.) mounting holes at both ends for easy installation on RC members, as presented in Figure 11-C. To facilitate the installation of the extensions and ensure that the extensions are properly attached, a jig was purchased to align the extensions to the ST350. This is done prior to installing the ST350s to the concrete. This makes the installation procedure simpler and quicker.

The recommended gauge extension length used for the test is a function of the member type, member depth, and span length. Table 1 provides guidelines for choosing the appropriate gauge length based on these parameters.

Table 1. Ext. Multiplier for Recommended Gauge Extension Length

Recommended	Lower and Upper Gage	Limits
Structure Type	Lower Limit	Upper Limit
Slabs & Rectangular Beams	1.0 × Depth of Member	Length of Span / 20
T-Beams	1.5 × Depth of Member	Length of Span / 20

After obtaining the appropriate gauge length, the measurements must be reduced to account for the extension effects on the readings. The new reading can be determined from the equation in Figure 12:

$$Reading = \frac{Reading}{Ext.\,Multiplier} \times Amplification\ Factor$$

Figure 12. Equation. Equation for extension effects.

where the amplification factor is taken as 1.1 to account for the extension effect and the Ext. Multiplier is given in Table 2.

Table 2. Corresponding Ext. Multiplier and Amplification Factor for Desired Gauge Length

Gage Extension Length	Ext. Multiplier	Amplification Factor
6 in.	2	1.1
9 in.	3	1.1
12 in.	4	1.1
15 in.	5	1.1
18 in.	6	1.1
21 in.	7	1.1
24 in.	8	1.1

To minimize the force on the ST350s, BDI recommends keeping the maximum strain below ±1,000 με. There are also maximum strain ranges that depend on the extension and properties of the concrete. These maximum values are provided to ensure accuracy for the given gauge length. Greater strain values can be measured. However, BDI suggests that special attention be given to the gain settings on the DAQ being used when exceeding these ranges. These maximum strain ranges are provided in Table 3.

Table 3. Maximum Strain Gauge Range for Concrete and Gauge Length

Ext. Mult.	Actual Gage Length with Extension	Maximum Strain Range	Approx. Conc. Stress for F'c = 20.7 MPa (3,000 psi)	Approx. Conc. Stress for F'c = 27.6 MPa (4,000 psi)	Approx. Conc. Stress for F'c = 34.5 MPa (5,000 psi)	Approx. Steel Rebar Stress
1	76.2 mm (3 in.)	±1000 με	21.4 MPa (3.1 ksi)	24.8 MPa (3.6 ksi)	27.6 MPa (4.0 ksi)	207 MPa (30 ksi)
2	152.4 mm (6 in.)	±500 με	11.0 MPa (1.6 ksi)	12.4 MPa (1.8 ksi)	13.8 MPa (2.0 ksi)	103 MPa (15 ksi)
3	228.6 mm (9 in.)	±330 με	6.9 MPa (1.0 ksi)	8.3 MPa (1.2 ksi)	9.0 MPa (1.3 ksi)	68.3 MPa (9.9 ksi)
4	304.8 mm (12 in.)	±250 με	5.3 MPa (780 psi)	6.2 MPa (900 psi)	6.9 MPa (1.0 ksi)	51.7 MPa (7.5 ksi)
5	381.0 mm (15 in.)	±200 με	4.3 MPa (625 psi)	5.0 MPa (720 psi)	5.5 MPa (800 psi)	41.4 MPa (6.0 ksi)
6	457.2 mm (18 in.)	±160 με	3.4 MPa (500 psi)	4.0 MPa (575 psi)	4.5 MPa (650 psi)	33.1 MPa (4.8 ksi)
7	533.4 mm (21 in.)	±140 με	3.0 MPa (440 psi)	3.4 MPa (500 psi)	3.9 MPa (560 psi)	29.0 MPa (4.2 ksi)
8	609.6 mm (24 in.)	±125 με	2.7 MPa (390 psi)	3.1 MPa (450 psi)	3.4 MPa (500 psi)	26.2 MPa (3.8 ksi)

The STS4 system is not complete without a laptop computer for data visualization and processing. BDI provides some recommendations for computer requirements. The computer used for the testing was equipped with an Intel Core i7 processor and 16 GB RAM. The computer has 512 GB SSD internal storage capacity. It also has up to 13 hours of battery run time. Windows 10 Pro was installed and recommended by BDI for using their software applications. The computer will run BDI's STS-LIVE software, which is used for visualizing the sensor readings during the test. The computer was also equipped with the BDI's STS-VIEW software for post-processing the results.

CHAPTER 3: PIATT COUNTY BRIDGE TEST

BRIDGE DESCRIPTION

The first bridge considered in this study was a 7 m (23 ft) two-lane, single-span RC slab bridge constructed in 1925 in Piatt County, Illinois. Figure 13-A presents an image of the bridge, and Figure 13-B illustrates its dimensions in plan view with a cross-sectional view of the slab and RC barriers. The bridge was chosen because of its proximity to the University of Illinois campus, availability of the design drawings, old age, and low RF. The bridge slab varies in depth from 0.3 m (12.5 in.) at the face of the curb to 0.4 m (15.5 in.) at the crown with 0.5 m (19 in.) wide curbs and integral RC railings. The slab has a total width of 9.8 m (32.2 ft) perpendicular to the direction of traffic and has a 24-degree skew angle. The design drawings indicate the slab was made of standard IDOT Class A concrete specified prior to 1930, which has a compressive strength equal to 20.7 MPa (3,000 psi). The diameter of the primary longitudinal reinforcing bars was 28.7 mm (1.13 in.) A coring sample test was conducted in 2007 to test the compressive strength of the concrete slab. Test results indicated an average compressive strength of 55.7 MPa (8,077 psi).

During a field inspection, spalling of the concrete slab was noticed along the southeast abutment in several locations, fully exposing the reinforcement. Figure 13-B presents the spalling of the bottom slab, as indicated by the hatched areas in the plan view of the bridge. More spalling was evident along the southwest portion of the slab and spanning the south lane in the longitudinal direction. Figure 13-C presents photographs of the damage corresponding to locations (1), (2), and (3) displayed in Figure 13-B.

A. Bridge photograph

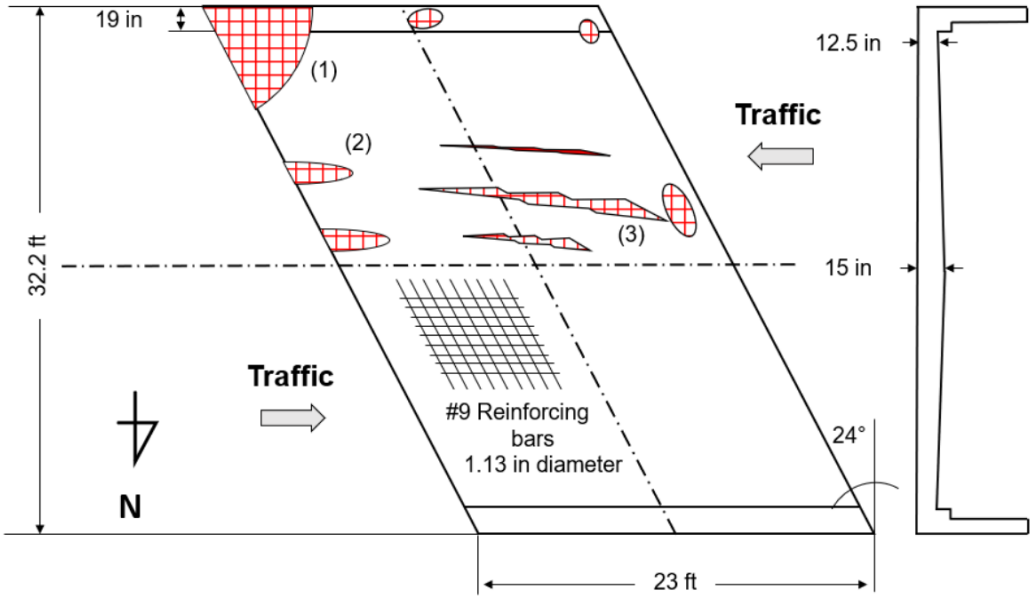

B. Plan view illustrating localized damage and section view showing cross section

C. Photographs of the damage

Figure 13. Photo. Tested bridge in Piatt County, Illinois.

During a field inspection, spalling of the concrete slab was noticed along the southeast abutment in several locations, fully exposing the reinforcement. Figure 13-B presents the spalling of the bottom slab, as indicated by the hatched areas in the plan view of the bridge. More spalling was evident along the southwest portion of the slab and spanning the south lane in the longitudinal direction. Figure 13-C presents photographs of the damage corresponding to locations (1), (2), and (3) displayed in Figure 13-B.

ANALYTICAL LOAD-RATING RESULTS

The live load effect that controlled the load-rating analysis was the positive moment at the midspan. The bridge was evaluated under a single lane load (SLL) and a multilane load (MLL) to determine which would produce the greatest load effects. The slab depth used in the analysis was 0.3 m (12.5 in.). The area of steel reinforcement was reduced by 10% when calculating the section capacity to

account for the localized delamination of the reinforcement observed during the inspection (Figure 13-C). The 10% reduction was assumed based on IDOT *Structural Services Manual* procedures and for direct comparison with the IDOT load-rating procedures (IDOT, 2017).

Table 4 summarizes the analytical RFs calculated using the concrete properties specified in the design plans and tested core samples. The MLL condition governed the load rating for the bridge. The analytical load rating improved by approximately 11% when applying the tested concrete properties in the analysis. These properties are used for subsequent calculations.

Table 4. Analytical Load Rating for Piatt County Bridge Using Design and Tested Concrete Properties for Single Lane Load and Multilane Load

Lane Loading	AASHTO LFR Using Design Properties	AASHTO LFR Using Tested Properties
SLL	0.588	0.655
MLL	0.519	0.578

DIAGNOSTIC TEST SENSOR PLAN AND LOADING PLAN

The STS4 instrumentation was chosen for this project because of its robustness, simple setup, and wireless sensor network. Nine strain gauges, labeled S1 through S9 in Figure 14, were distributed incrementally along the critical section of the bridge and oriented to capture the longitudinal strain profile from the test truck loads. The strain gauges were mounted using 0.3 m (12 in.) gauge extensions and concrete studs, which were embedded into the slab.

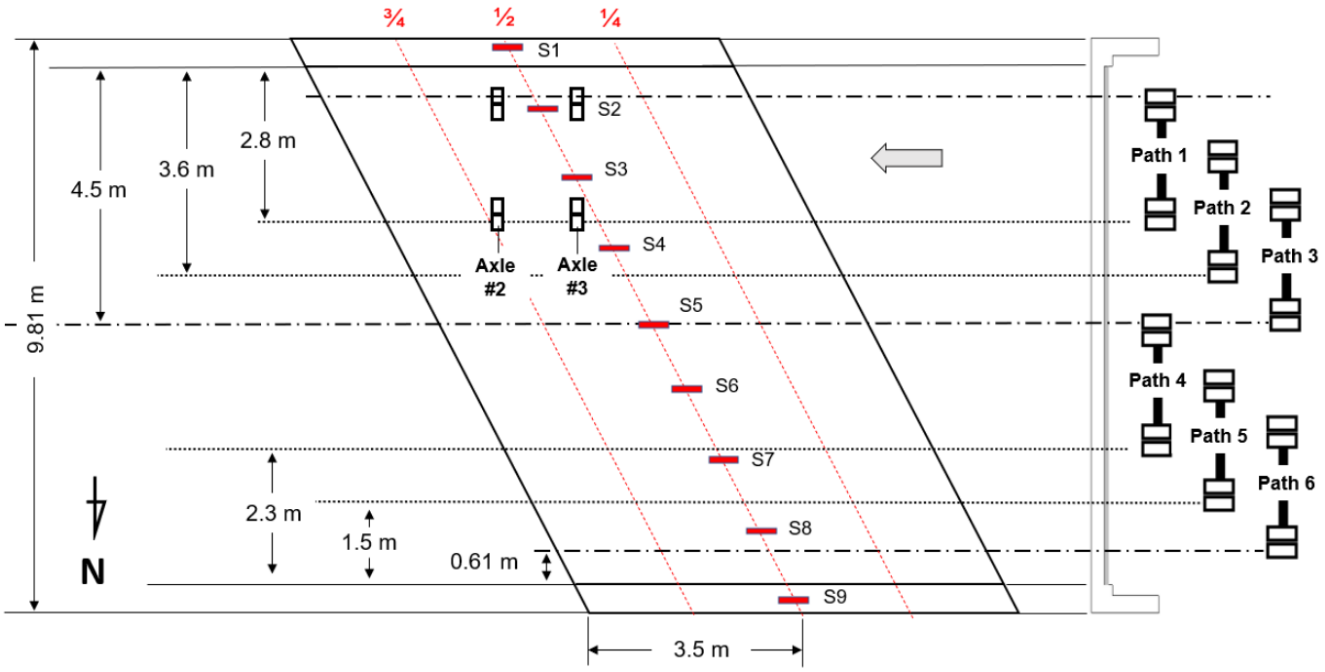

Figure 14. Illustration. Strain gauge and loading plans for the diagnostic test of Piatt County bridge.

A single truck was used for the diagnostic test for two reasons. The first was to avoid long detours to the immoderately trafficked route, and the second was due to the sufficiency of a single truckload to provide a reasonable assessment of the condition of the bridge in preparation for the proof load test. The truck selected for this test was a conventional IDOT dump truck with an axle configuration presented in Figure 15. The truck was loaded such that its effect on the bridge was approximately 60% of the maximum HS-20 bending moment. This load is sufficiently high to prevent any damage to the bridge and produce responses along the transverse width that can be measured accurately by the sensors. The test truck axle loads were measured using movable scales just prior to loading the bridge. Because of the short span of the bridge, only the rear tandem axle fits on the bridge span to produce the desired load effect. Hence, only the rear tandem axle loads, presented in Figure 15-B, were relevant for the analysis.

A. Truck photograph

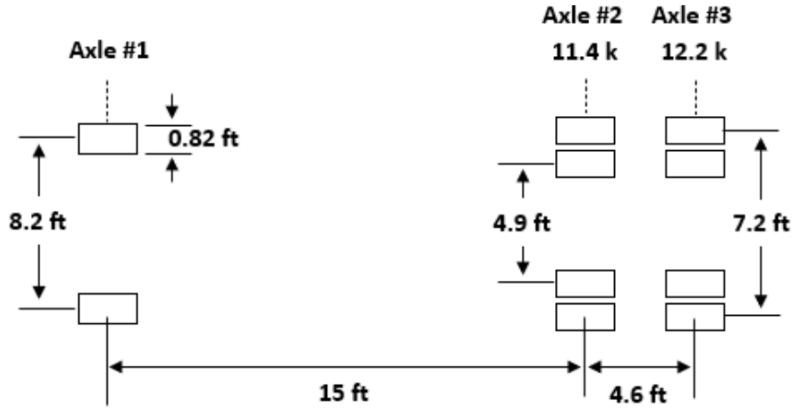

B. Plan-view dimensions of wheel and axle configuration showing measured axle loads

Figure 15. Illustration. Test truck used for the diagnostic test of Piatt County bridge.

As presented in Figure 14, the loading plan comprised of six truck paths in the traverse direction of the bridge. The bridge was loaded in a quasi-static manner, where the truck crosses the bridge at a crawling speed of about 2.2 m/s (5 mph). This allows numerous loading conditions to be recorded along the bridge for each truck pass, covering most of the bridge loading conditions in a relatively short amount of time. Each path was repeated three times to ensure the reliability of the measured

responses. The tandem axle position presented in the plan view of Figure 14 produced the maximum load effects recorded during the field test. The dotted transverse skew lines represent the quarter points of the span, and the arrow represents the direction the truck traveled for all load paths.

DIAGNOSTIC TEST LOAD-RATING RESULTS

The maximum measured member strain (ϵ_T) occurred along path 1 when the north side of axle #2 of the truck coincided with the three-quarter section of the bridge, as presented in Figure 14. Because the strain gauges producing the maximum recorded values were located along the south edge of the slab, the edge strip section presented in Figure 16 was used to approximate the appropriate section factor resisting the applied load (AASHTO, 2018). The section factor includes the portion of slab, curb, and integral RC railing contributing to the stiffness of the element. This assumption was made based on previous research, which has shown the edge beam to contribute significantly to the moment distribution along the edges of RC slab bridges (Azizinamini et al., 1994; Amer et al., 1999; Mabsout et al., 2004). The width of the edge strip was determined from Figure 3, representing the distribution width of a single line of wheels for the rating vehicle. The response at S1 was assumed to be resisted by the edge beam, which consisted of the integral curb and RC railing (AASHTO, 2002). Therefore, only the peak strain value from S2 beneath the slab (see Figure 16), i.e., the response recorded by the first interior strain gauge, was used for the calculation of K_a. Applying Figure 7, a K_a value equal to −0.310 was obtained, implying a reduction in load capacity from the analytical results.

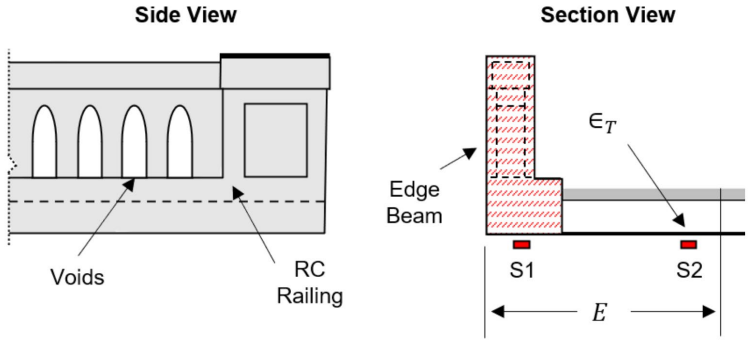

Figure 16. Illustration. Side-view railing detail and cross section considered for calculating K_a.

The K_b factor was obtained using the cracking strain of the concrete as a threshold to determine if the linear behavior of the bridge could be extended to a load level of 1.33 W, as defined in the *MBE* (AASHTO, 2018). A strain limit of 132 μϵ was calculated using the tensile strength of the concrete. The theoretical strain calculated for the applied truck load was greater than the strain limit, yielding a K_b factor equal to 0. This finding indicated that there would be no enhancement to the load rating of the bridge from the field test. Plugging the factors into Figure 5 and Figure 6 returns a modified RF of 0.655, showing no improvement from the analytical RF.

LOAD RATING USING CALIBRATED MODEL

The 1D beam line model used for the analytical load rating was calibrated based on the diagnostic test results to obtain a modified RF for the MLL case. To calibrate the model, the material properties

of the section presented in Figure 17 were adjusted to match the results of the maximum measured strain (ϵ_T) during the field test. The expression in Figure 17 was used to calculate the modified modulus of elasticity E of the concrete:

$$E = \frac{M}{S\,\epsilon_T}$$

Figure 17. Equation. Equation for modulus of elasticity.

LOAD RATING USING STRUCTURAL EFFECTIVE STRIP WIDTH APPROACH

The calculated moment distribution from the diagnostic test was used to determine a modified EW for the bridge. The critical moment distribution is illustrated in Figure 18, showing the cross-sectional location of the truck axles relative to the edge of the curb. The moments between the discrete sensor values were assumed to be linear. Moreover, the sum of the moments under the curve was assumed to be equal to the externally applied moment from the idealized truck load (Arockiasamy & Amer, 1997). As discussed earlier, the edge beam strain values were neglected, leaving just the shaded region in Figure 18 under consideration in the analysis. Because the edge beam moment was neglected, the peak moment for this case was taken as 7.1 kN-m/m (1.6 kip-ft/ft) and located approximately 1.4 m (4.6 ft) from the outer edge of the bridge. The area of the shaded region was then divided by this value to determine the modified EW for the bridge.

The modified structural EW calculated from the diagnostic load test was equal to 3.4 m (11.3 ft). The measured EW was 5% more than AASHTO's, indicating that a larger portion of the slab was resisting the applied moment and that less stress was being imposed in the longitudinal direction of the slab. Consequently, the load rating for the SLL case also increased to 0.711 from the analytical RF computed using AASHTO.

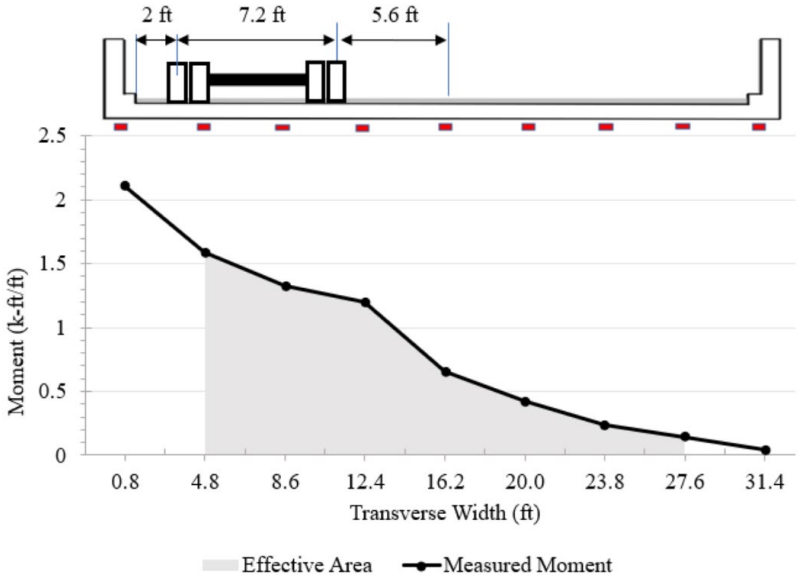

Figure 18. Graph. Moment distribution for critical load path from the diagnostic test of Piatt County bridge.

PROOF LOAD TEST SENSOR PLAN AND LOADING PLAN

For the proof load test, the strain gauges were kept in the same position and orientation as for the diagnostic load test (see Figure 14). As presented in Figure 19, eight linear variable differential transformers (LVDTs), labeled L1 through L8, were placed at the same location as the strain gauges along the critical section to capture the displacement profile in the transverse direction during testing. Figure 19 presents a plan view of the fixture used to support the LVDTs as well as a picture of the fixture taken under the slab bridge during the proof load test.

For multilane bridges, at least two lanes are required to be loaded during the proof load test (AASHTO, 2018). A target proof moment of 2896 kN-m/m (651 kip-ft/ft) was calculated using Figure 9. This value accounts for an ADTT below 1,000 (−10%) and considers that the bridge is a nonredundant structure (+10%). Moreover, because IDOT performed an in-depth inspection, X_p in Figure 8 was reduced by 5%.

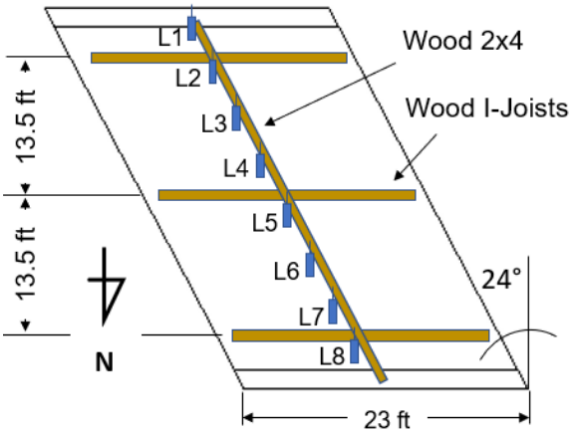

A. Plan view

B. Photograph of the fixture with installed LVDT sensors

Figure 19. Photo. LVDT distribution and the fixture constructed using wood I-joists for proof load test of Piatt County bridge.

Conducting the proof load test required the bridge to be closed. To avoid added costs and complications associated with extending the proof test to multiple days, the load testing was organized to last a single day. Because of constraints with test truck dimensions and loading capacities, it was not possible to load the bridge using the truck used for diagnostic testing. Preliminary calculations were necessary to determine an adequate and safe testing mechanism for loading the bridge to the required magnified loads. Furthermore, the loading would need to be easily adjustable to allow for incremental loading steps that are neither too large nor too small.

A 275 ton capacity crane was chosen to load the bridge in incremental loading stages using 98 kN (22 kip) stackable slab loads positioned directly on the bridge. Figure 20-A presents an image of the crane and the slab loads used for loading the bridge. Figure 20-B illustrates the plan-view configuration of the slab loads being transferred by wood oak boards beneath the slabs to load the bridge. The boards were 1.2 m (4 ft) in length and 152 mm (6 in.) wide. They were spaced such that they represent HS-20 axle spacing in the transverse direction 1.8 m (6 ft) and spaced 1.2 m (4 ft) from each other between lanes. The transverse positioning of the slab pair was decided based on varying the configuration along the transverse width and finding the location that produced the maximum effects. This transverse positioning of the oak boards was then fixed for the remainder of the test. The loading stages began with one slab load in each lane positioned on the bridge to produce a theoretical moment that is 25% of L_T as determined from the preliminary 1D beam line analysis. The loading was amplified in subsequent stages by adding a combination of more slab loads and shifting the position of the loads toward midspan. Each loading stage was repeated two times to assess the consistency of the measured responses.

A. Photographs of the crane

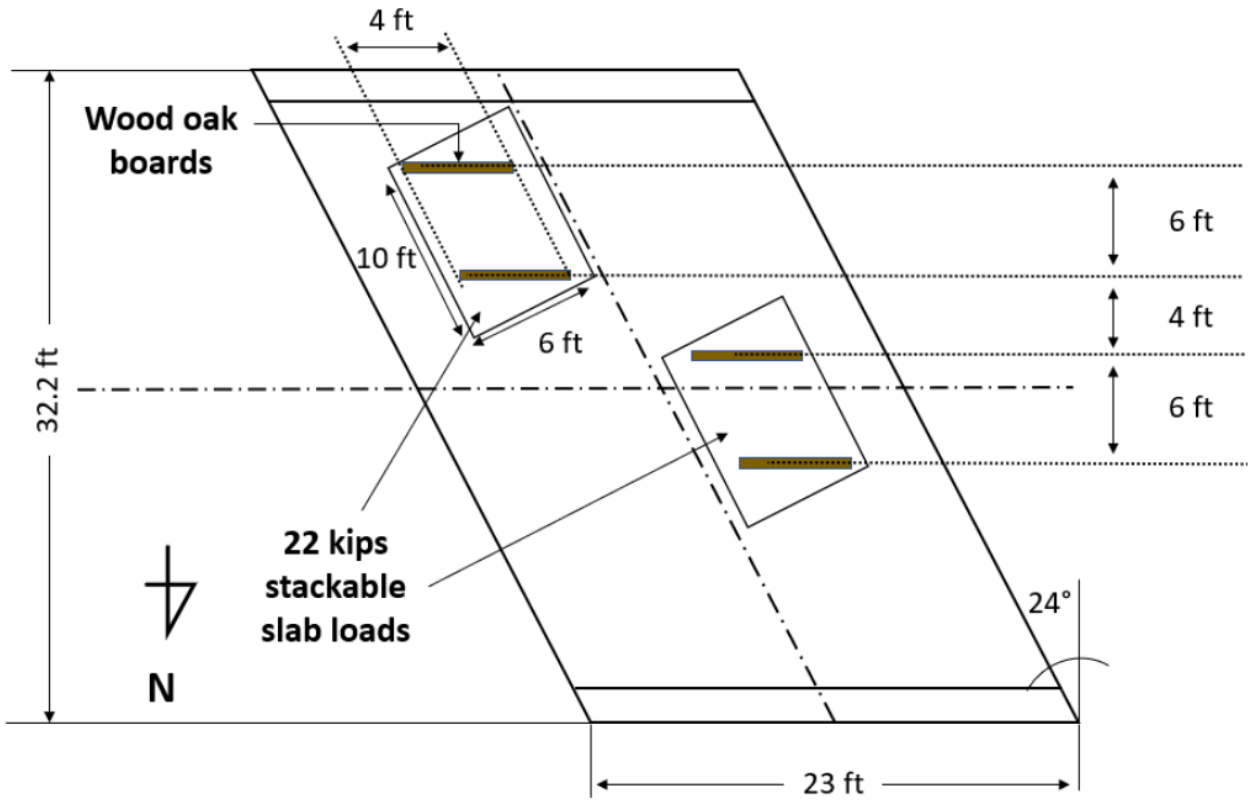

B. Plan-view configuration of slab loads and wood oak boards used to transfer the loads

Figure 20. Illustration. Loading crane and loading plan for proof load testing of Piatt County bridge.

PROOF LOAD TEST LOAD-RATING RESULTS

Data processing for the proof load test was performed with the sensor results exported directly from the BDI STS-LIVE software. Figure 21 presents a plot of the response histories for the critical LVDTs and strain gauges recorded during the proof load test. The figures were processed in the STS-VIEW software where the data can be visualized quickly as a function of time. Both run 1 and run 2 of stage 3 are presented in the plots. Also presented in the plots are the time-stamped data points denoted by the trapezoidal shapes on the figures. These are the points just prior and after the slab loads were placed on the bridge. These points were added during the load test using the comment feature of the STS-LIVE software. The peak responses processed for the load-rating evaluation were the instantaneous sensor responses. These were the points just after the slab loads were placed on the bridge. Some time-dependent displacements and strains were apparent from the plots. However, these are attributed to other effects such as the wind's influence on the sensors, which was not relevant to the load-rating analysis.

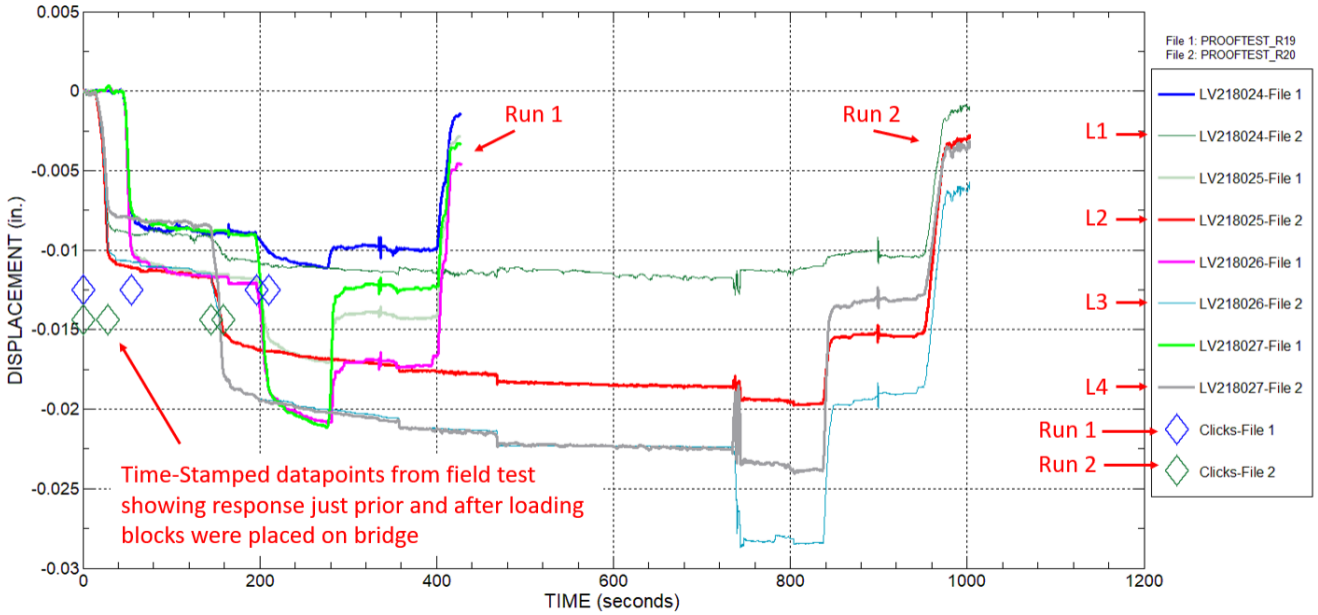

A. Displacement response history plot for L1 through L4

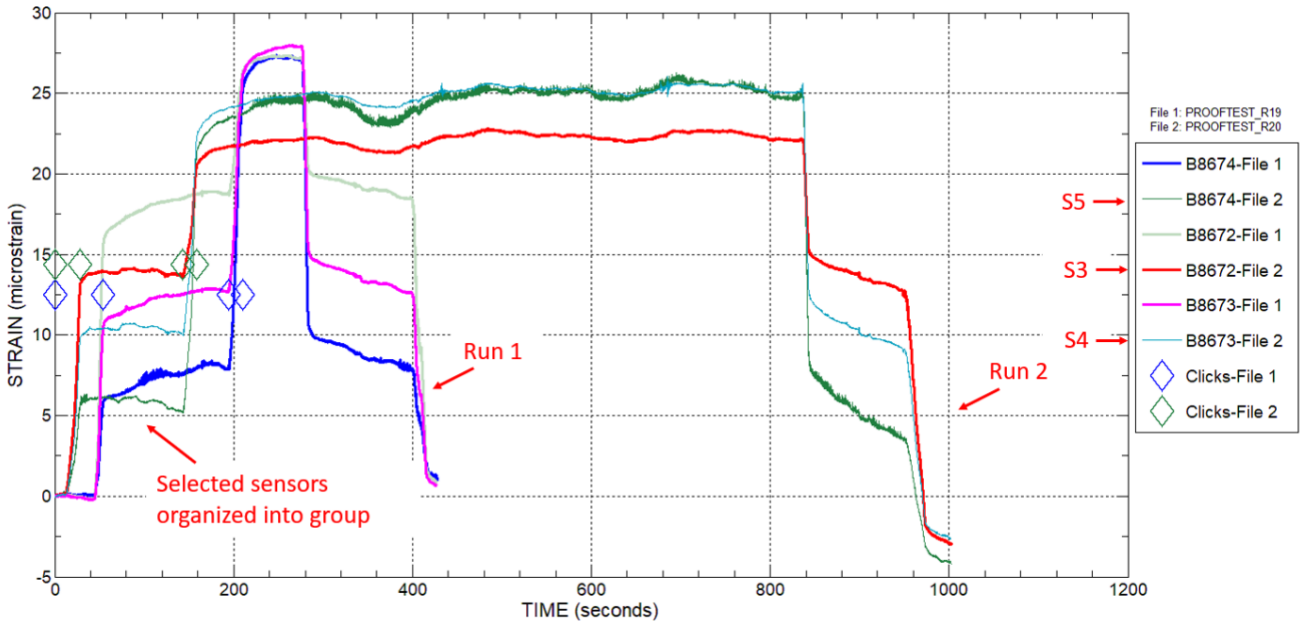

B. Strain response history for S3 through S5 recorded in STS-LIVE for run 1 and run 2 of stage 3 loading of the proof load test

Figure 21. Graph. Data plots for proof load test of Piatt County bridge.

Figure 22 presents a plot of the displacement history including the residual displacements for LVDT 3 producing the peak values on the bridge. This plot helps illustrate the loading sequence, the difference between each loading run, and the residual displacements upon unloading for every loading step. At stage 1 loading (25% L_T), the two bridge runs were nearly identical with no residual

displacements upon unloading. A residual displacement approximately equal to 10% was observed for run 1 of stage 2 loading (50% L_T). However, when the loading was repeated for run 2, there was no increase in the residual displacement and the peak displacements were almost equal. The displacement increased by 5.5% for run 2 compared to run 1 of stage 3 (67% L_T), implying the bridge was displacing more than anticipated for the applied theoretical moment. Moreover, a residual displacement of approximately 12% was observed during the final run of stage 3, leading to the conclusion that the bridge has undergone some permanent deformation. Hence, the researchers terminated the test after the second run of stage 3. Because the observed distress occurred during stage 3 loading, AASHTO requires that the L_p used in Figure 10 be the load just prior to reaching the load causing distress in the bridge. Applying Figure 10 with a k_0 equal to 0.88 and an L_p corresponding to the stage 2 loading, a modified RF equal to 0.425 was calculated, which is 26% less in load rating compared to the analytical results.

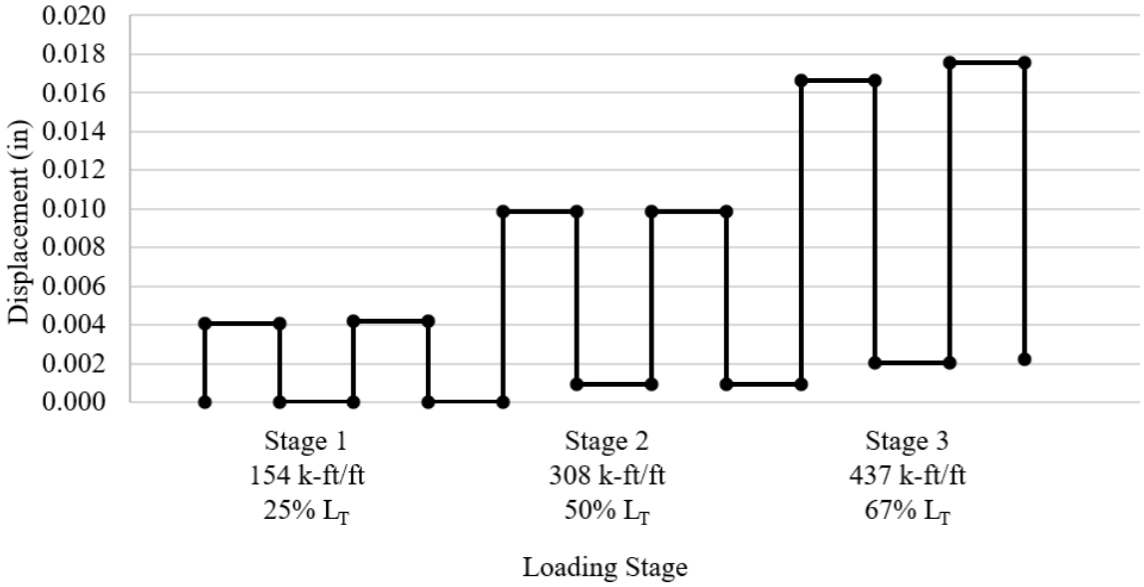

Figure 22. Graph. Load-displacement history for proof load test recorded by LVDT 3.

LOAD RATING USING STRUCTURAL EFFECTIVE STRIP WIDTH APPROACH

Figure 23 presents the transverse moment distribution from the proof load test for the critical load case. The figure also illustrates the location of the loads along the transverse width of the bridge producing the maximum effects. The peak strain value was observed under the south edge beam as predicted from studying the diagnostic test results. No strain gauge was placed under the north curb of the bridge because of limitations in the number of data channels available for the test. It was therefore conservatively assumed to be zero. The structural EW was determined as 2.8 m (9.13 ft), which is 3% less compared to the effective width calculated using Figure 3. The resulting modified RF for the MLL case was calculated as 0.560.

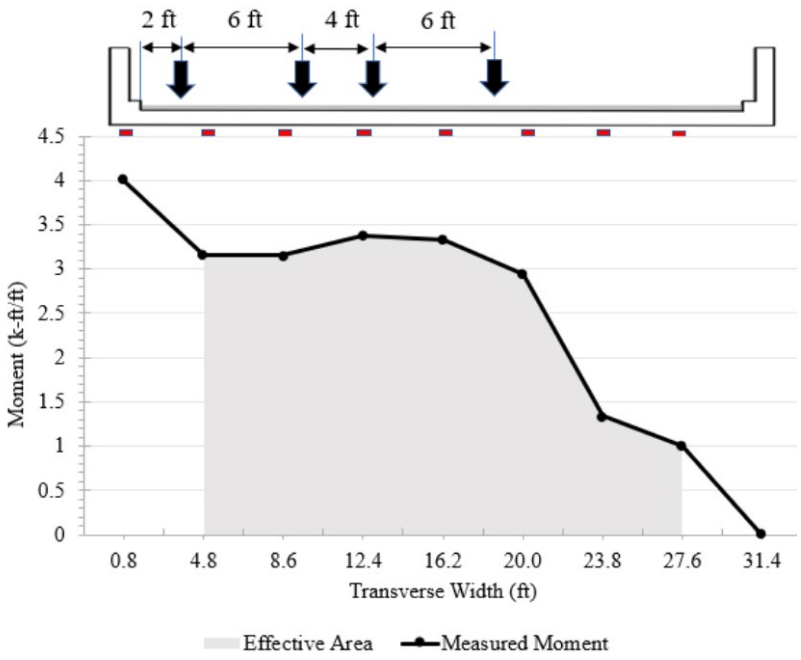

Figure 23. Graph. Moment distribution for critical load path from the proof load test of Piatt County bridge.

RESULTS COMPARISON AND DISCUSSION FOR PIATT BRIDGE TEST

Table 5 presents a summary of the load-rating results. The modified RF using the diagnostic load test MBE procedure suggests the test results cannot be extrapolated directly to performance at greater loads, although the calculated K_a factor shows the load effects on the bridge were more significant than those obtained from the theoretical model. The modified RF using the diagnostic test EW approach shows an improvement from the analytical RF by about 8%. This result was not representative of the actual rating because the test was conducted under SLL. An MLL diagnostic test would give a better approximation of the modified load capacity for the bridge. Furthermore, neglecting the edge beams, skew angle, and the effects of SLL in the analysis distorts the effective width calculations and final RF. The modified RFs using the diagnostic test calibrated model and the proof load test approaches give better estimations of the bridge load capacity and condition. Results show that the load rating for the critical MLL case decreased by as much as 26% in the case of the proof load test using the MBE approach, by about 16% using the calibrated model, and by about 3% using the EW approach.

The calibrated model resulted in a 32% improvement in the RF compared to the MBE proof load test. Although both EW and MBE methods using the proof test resulted in smaller RFs compared to that of the analytical approach, the MBE approach proved to be more conservative than the EW approach, showing a 26% smaller RF compared to the EW approach. This was also evident in the diagnostic test results, where the MBE approach gave an 8% smaller RF than that computed using the EW approach. When compared to the MBE methods, the EW approach was more involved, requiring each strain measurement along the cross section of the bridge to be considered to compute an EW for the bridge. The MBE procedure was straightforward, simply requiring the peak strain of the critical load

case to be used in the diagnostic test analysis and the maximum applied live load (L_p) for the proof load test analysis.

The reductions in load rating are attributed to the significant damage observed on the bridge. The localized damage under the south curb and extensive longitudinal cracks observed during the visual inspection significantly altered the load distribution in the slab. Moreover, the modified load ratings presented in Table 5 illustrate that more conservative analytical load ratings may be necessary for older RC slab bridges that have noticeable damage and unique geometric properties.

Table 5. Summary of Modified Load Ratings Using Different Methods

Load-Rating Approach		Modified RF	Analytical RF	Loading Type
Diagnostic	EW	0.711	0.655	SLL
	MBE	0.655		
Proof	EW	0.560	0.578	MLL
	MBE	0.425		
Calibrated Model		0.488		

CONCLUSIONS OF PIATT COUNTY BRIDGE TEST

This study used several analytical and experimental methods to present a load-rating analysis on an old RC slab-skewed bridge. Diagnostic and proof load testing were employed on the bridge for calculating modified RFs to compare with the AASHTO analytical load-rating results. Two approaches—namely, AASHTO's MBE approach and the EW approach—were applied and discussed for each load test. A summary of the main findings of this bridge study are as follows:

- Load testing may reduce the load ratings for RC slab bridges that have noticeable damage and unique geometric properties. In such cases, conservative assumptions may be necessary when estimating the material properties and section properties of the concrete slab for load rating similar bridges.

- The MBE approach gave more conservative load ratings showing a 14% and 31% smaller RF compared to the EW approach for the diagnostic test and proof load test, respectively.

- The load rating for the bridge was reduced by an average of 26% using the SLL diagnostic test MBE and EW approaches compared to the analytical load-rating procedure.

- The controlling load rating for the bridge was reduced by an average of 24% using the MLL calibrated model and proof load test MBE and EW approaches compared to the analytical load-rating procedure.

- The calibrated 1D beam line model from the SLL diagnostic test conveyed a 25% greater RF than that calculated using AASHTO's MBE proof test procedure and a 13% lesser RF than

calculated using the EW approach. This finding shows that the calibrated model can be used to estimate a reasonable load RF for the bridge at greater load levels.

This load-rating study demonstrates that bridge load rating can vary by as much as 38% depending on the method employed for the load-rating analysis. Load rating using the MBE approach was simpler to apply, while the EW approach was less conservative. The diagnostic and proof load testing procedures used on the bridge were expensive compared to the analytical rating procedure.

CHAPTER 4: MCLEAN COUNTY BRIDGE TEST

BRIDGE DESCRIPTION

The second bridge considered in this study was in McLean County, Illinois (Figure 24). The bridge, constructed in 1954, was decommissioned and scheduled for replacement because of its age and load posting. The tested bridge was a two-lane continuous two-span RC slab bridge with span lengths of 9.8 m (32 ft), a width of 7.3 m (24 ft), and 0.3 m (12 in.) wide curbs. The design drawings specify a concrete compressive strength equal to 24 MPa (3,500 psi) and 32.2 mm (1.27 in.) diameter longitudinal rebars. A coring sample test was performed for the slab, resulting in an average compressive strength of 30 MPa (4,450 psi). The bridge had several longitudinal microcracks along the bottom of the slab and a long transverse crack located about 3.81 m (12.5 ft) from the abutment face.

Figure 24. Photo. McLean County bridge.

ANALYTICAL LOAD-RATING RESULTS

The analytical load RFs were determined using the concrete properties specified in the design plans and tested core samples (Table 6). The load rating was controlled by the MLL condition along the positive moment region located 3.4 m (11 ft) from the abutment face. Although the bridge capacity was reduced along the negative moment region where there was a discontinuity in the primary reinforcement, the dead load effects were much less significant in this region, leading to the controlling load rating in the positive moment region. The analytical load rating improved when applying the tested concrete properties in the analysis. These properties are used in subsequent calculations.

Table 6. Analytical Load Rating for McLean County Bridge

Critical Section	Lane Loading	AASHTO LFR Using Design Properties	AASHTO LFR Using Tested Properties
Positive Moment	SLL	0.925	0.946
	MLL	0.858	0.879
Negative Moment	SLL	0.969	0.991
	MLL	0.899	0.920

DIAGNOSTIC TEST SENSOR PLAN AND LOADING PLAN

Eight strain gauges, labeled S1 through S8 in Figure 25, were positioned incrementally along the critical section. The instrumentation was the same used for the previous bridge study and oriented to capture the longitudinal strain profile for the bridge under diagnostic test loading. The strain gauges were attached using a stud mounting technique with 0.5 m (18 in.) gauge extensions. The tested span was chosen based on inspection of the bridge. The north span had more extensive cracks, including a 4 m (13 ft) transverse crack close to the critical section. Furthermore, the span was more convenient for sensor installation and testing purposes.

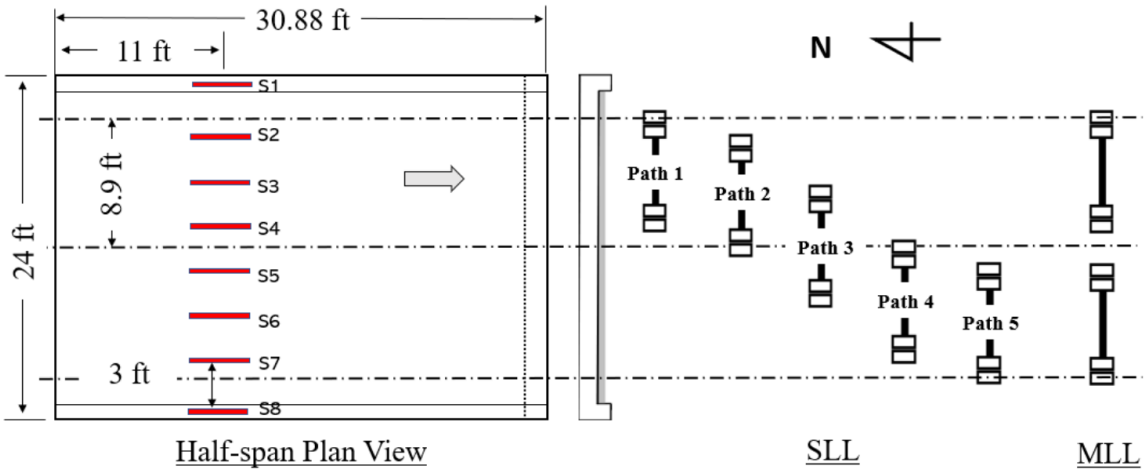

Figure 25. Illustration. Half-span plan view of McLean County bridge showing the strain gauge sensor configuration and load paths for SLL and MLL.

Both SLL and MLL were considered for the diagnostic test loading conditions to obtain an RF from the diagnostic test for the controlling MLL case. Figure 26 presents the trucks selected for this test. Truck 1 was used for the SLL case. The trucks were loaded such that their effect on the bridge was approximately 80% of the maximum HS-20 bending moment to allow for a modified load rating from the test results regardless of whether the bridge behavior cannot be extrapolated to the amplified loads of 1.33 W specified in the AASHTO *MBE* (2018). The test truck axle loads were measured using movable scales prior to loading the bridge. Figure 26-B presents the measured axle loads.

A. Image of the trucks

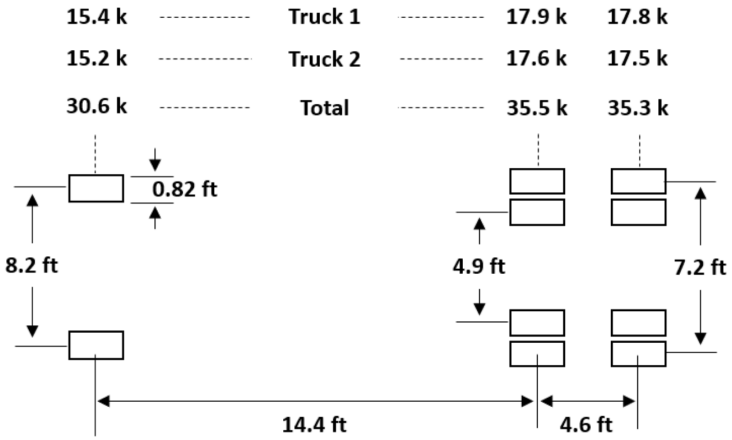

B. Plan-view axle configuration with measured axle loads for both trucks

Figure 26. Illustration. Loading trucks for the diagnostic test of McLean County bridge.

As presented in Figure 25, the loading plan comprised of five truck paths in the traverse direction of the bridge under SLL and one truck path under MLL. The bridge was loaded with the trucks going at a crawl speed of approximately 5 mph (2.2 m/s). Each path was repeated two times to ensure the reliability of the measured responses. The truck path producing the greatest load effects under SLL was along path 3 at S4. The maximum response under MLL was also at S4. The trucks traveled south for all load paths.

DIAGNOSTIC TEST LOAD-RATING RESULTS

The maximum measured member strain (ϵ_T) used for post-processing occurred at S4, when the first of the rear tandem truck axles crossed over the critical section of the bridge. The section factor assumed to resist the applied load was based on the properties of the slab. Applying Figure 7, a K_a value equal to 0.89 was obtained, implying an improvement in load capacity from the analytical results.

The K_b factor was obtained using the cracking strain of the concrete as a threshold to determine if the linear behavior of the bridge could be extended to a load level of 1.33 W. A strain limit of 132 με was calculated using the tensile strength of the concrete. The theoretical strain calculated for the applied truck load was greater than the strain limit, yielding a K_b factor equal to 0.5 since the truck load was sufficiently high to obtain some meaningful results from this load test (AASHTO, 2018). Plugging the factors into Figure 5 and Figure 6 returns a modified RF of 1.27, indicating a 44% improvement from the controlling analytical RF.

PROOF LOAD TEST SENSOR PLAN AND LOADING PLAN

A fixture was constructed using wood I-joists to support the LVDTs along the critical location during the field test. The LVDTs were in the same positions as the strain gauges used for the diagnostic tests. The strain gauges were kept in the same position and orientation as for the diagnostic load test (see Figure 25). As presented in Figure 27, eight LVDTs, labeled L1 through L8, were positioned along the critical section to capture the displacement profile along the transverse direction during testing. Figure 27 presents a plan view of the LVDTs and strain gauges positioned on the north span and a picture of the fixture taken under the slab bridge during the proof load test.

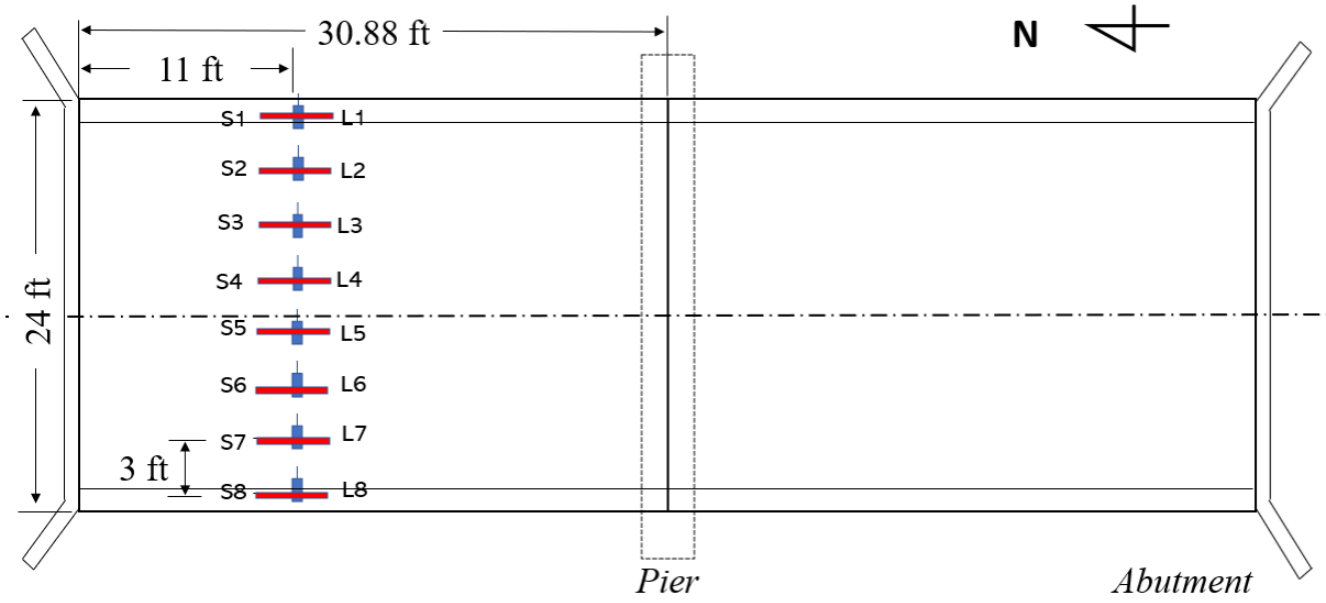

A. Plan view

B. Photograph of the fixture with sensors installed on bridge

Figure 27. Photo. Instrumentation plan for proof load test of McLean County bridge.

Conducting the proof load test required the bridge to be closed. The load testing was organized to last a single day using two trailer trucks that would be driven simultaneously onto the bridge as live loads. The trailer trucks were nearly identical with slight differences in the trailer bed length, which had a minor influence on the loading effects. The trailers were loaded using a small crawler crane that stacked the 14.2 kN (3,200 lb) bin blocks used for weights onto the trailer beds of the trucks. Figure 28-A presents an image of one of the trailer trucks used for the proof load test along with the crawler crane and bin blocks used for the test. The axle weights were measured on the field before loading the bridge using digital scales. Figure 28-B presents an image of the movable scales used for measuring the axle weights.

A. Concrete bin blocks used for weight and the crawler crane used to load the trailers

B. Movable scales used to measure axle loads during the proof load test

Figure 28. Photo. Image of one of the trailer trucks for McLean County bridge.

The location of the trucks that produced the maximum moment at the critical positive moment region of the bridge was determined from the 1D beam line analysis. Only the rear tandem axles of the test trucks were on the bridge span to generate this moment. A target proof moment (L_T) of 3189 kN-m/m (717 kip-ft/ft) was calculated using Figure 9. This value accounts for an ADTT below 100 (−15%) and considers that an in-depth inspection was performed on the bridge (−5%). The desired loading increments were then established based on the percentage of the target proof load. Figure 29 illustrates the bin blocks' arrangement on the trailers used for each loading stage and the corresponding applied moment on the bridge. The percentage of the target proof load is also presented in the figure. For example, at loading stage 8, there were six rows of bin blocks spanning the length of the trailer and three rows across the width of the trailer. There was an additional stack of bin blocks placed on top of the rear two rows of the trailer. The total quantity of bin blocks on each trailer was 24 for stage 8 loading. This produced an applied moment of 866 kN-m (639 kip-ft) equal to 89.2% of L_T. This was the maximum moment achieved during the proof load test used for modifying the RF. Each loading stage was repeated two times to assess the consistency of the measured responses by backing the trucks onto and off the bridge.

Loading	Quantity of Bin Blocks in each Row						Moment	% L_T
Stage 8	3	3	3	3	*6	*6	639 k-ft	89.2 %
Stage 7	3	3	3	3	*6	*5	573 k-ft	80.0 %
Stage 6	3	3	3	3	*5	*5	501 k-ft	70.0 %
Stage 5	3	3	3	3	3	*5	440 k-ft	61.5 %
Stage 4	3	3	3	3	1		365 k-ft	51.0 %
Stage 3	3	3	3	1			271 k-ft	37.8 %
Stage 2	3	3	3				173 k-ft	24.2 %
Stage 1	2	2					123 k-ft	17.2 %

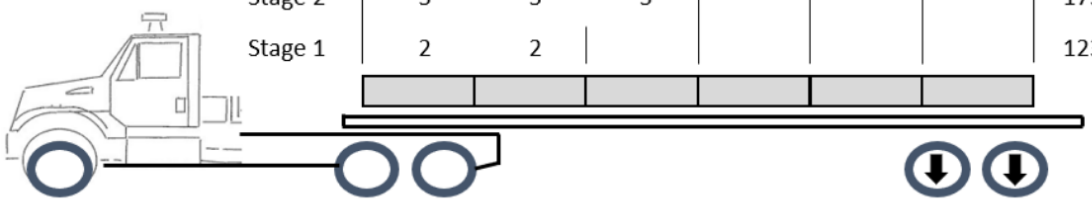

* Indicates bin blocks were also stacked on top (maximum 3 bin blocks along trailer width)

Figure 29. Illustration. Loading sequence for both trailers showing the number of bin blocks and the corresponding location on the trailer per loading stage during the proof load test of McLean County bridge.

PROOF LOAD TEST LOAD-RATING RESULTS

A spreadsheet using Microsoft Excel (2021) was created to evaluate the linearity of the bridge responses during the test. The results recorded in the STS-LIVE software were copied into Excel and processed between runs during the test. For each strain gauge, a plot of the magnitude with respect to the loading was generated. For each LVDT, a load-displacement plot was created, and a displacement history plot was created to show the residuals of the displacements after every loading stage. Figure 30-A presents a plot of the displacement history at LVDT 4 recorded during the proof load test. This LVDT recorded the largest displacements for the bridge during the proof load test. Figure 30-B presents a plot of the strain history for strain gauges S3, S4, and S5 recorded during the proof load test. As observed from the data, there were no significant signs of nonlinearity in the bridge response. There were some differences between runs. However, the residuals were all less than 10% of the measured response, indicating permanent deformation to the bridge. Also, the strain data never exceeded the estimated cracking strain of 132 $\mu\epsilon$. This estimated cracking strain is presented in Figure 30-B as a line representative of the limit where the measured strain of the slab has not exceeded the cracking strain. The strain gauge producing the maximum responses was S4, which was at the same location as L4.

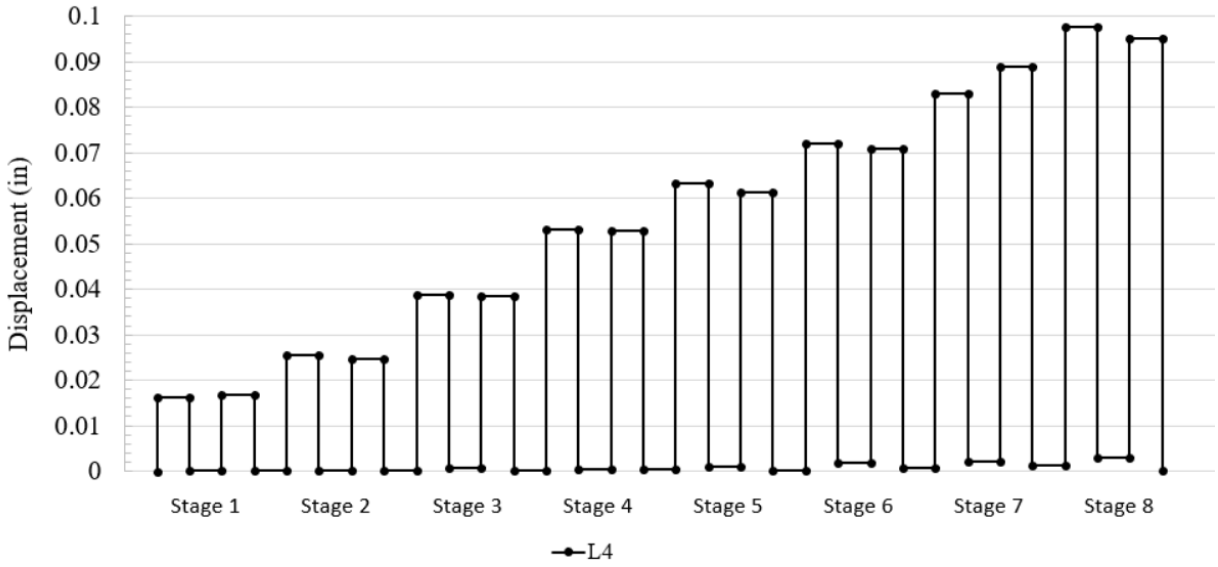

A. Displacement of LVDT 4

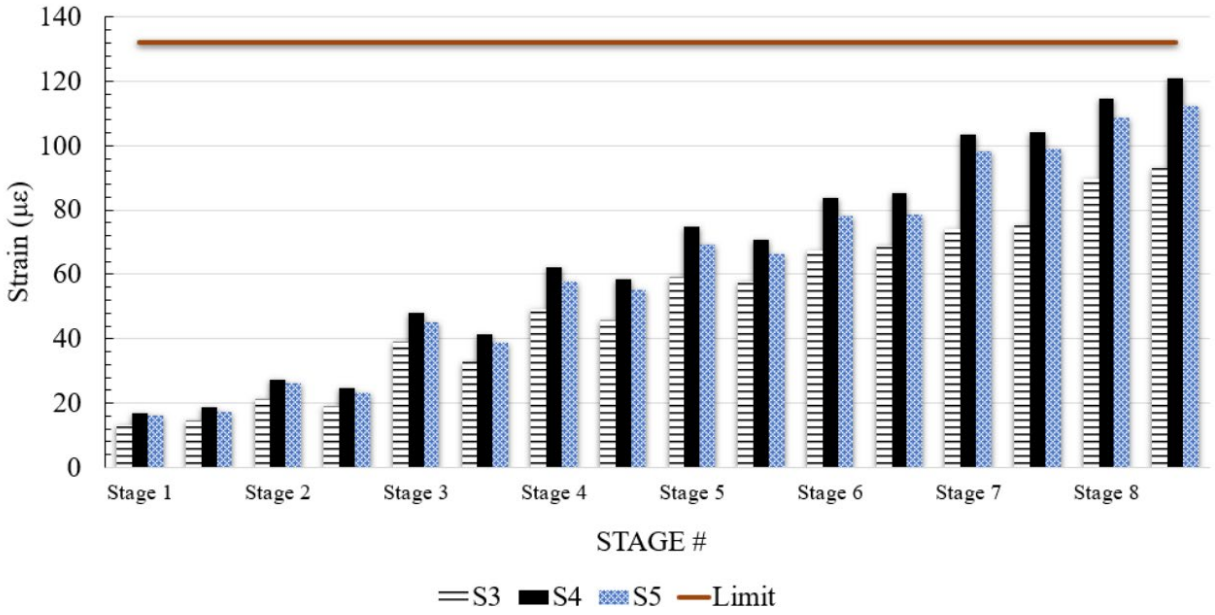

B. Strain gauge magnitudes of S3, S4 and S5

Figure 30. Graph. Proof load test response histories of McLean County bridge.

The proof load test was terminated after stage 8. No signs of distress in the bridge were apparent. However, the trucks were no longer capable of driving onto the bridge because of the heavy axle loads carving a large indentation into the roadway at the approach of the bridge. Figure 31 illustrates images of the roadway damage. Because the test was terminated due to nonstructural aspects of the load test and not because of observed distress in the bridge, the k_0 used in Figure 10 was taken as 1.0. A modified RF equal to 0.912 was calculated, which is a 4% improvement from the analytical results.

Figure 31. Photo. Damage to the road due to heavy axle loads during the proof load test of McLean County bridge.

RESULTS AND DISCUSSION OF MCLEAN BRIDGE TEST

Table 7 presents a summary of the load-rating results. The modified RF using the diagnostic load test MBE procedure suggests the bridge has a much greater load capacity than expected from the analytical load-rating results. The percentage improvement is as much as 44%. The modified RF using the proof load test shows only a minor improvement from the analytical RF of about 4%. The RF was not greater for the proof load test because of the need to stop the test earlier due to the damage on the roadway. Because there were no signs of distress in the bridge at nearly 90% L_T, the bridge is expected to carry the target proof load.

Table 7. Summary of RFs Computed for McLean County Bridge

Lane Loading	Analytical RF	Diagnostic Test RF	Proof Load Test RF
MLL	0.876	1.27	0.912

Overall, the field test results show that the bridge performed better than suggested by the analytical load rating. This shows that the analytical rating procedure using AASHTO LFD may give conservative RFs, which in this case, resulted in a load posting for the bridge that may not be necessary. Furthermore, the bridge was decommissioned and replaced, which could have been avoided or postponed to a much later time since the bridge has proven to show good performance under amplified loads. These expenditures could have been used for other more critical bridges in the Illinois bridge inventory, which is why these load tests are being investigated as an alternative load-rating method in this research.

Note that the EW approach and modified RF using a calibrated model were not performed for this study. The primary purpose of this study was to carry out the proof load test on the bridge and establish a loading protocol that can be used for subsequent bridge tests. The diagnostic load test was conducted under MLL, and the calibrated model was not necessary in this case for establishing a modified RF for the bridge. The results for the modified RFs using the EW procedure were not consistent with the results obtained using the AASHTO MBE method. The narrow width of the bridge combined with the MLL of the trucks during both load tests resulted in much smaller effective widths for the bridge. This is because the area under the moment distribution curve is much smaller with a narrow width, which yields a smaller EW result in the calculation. This analysis was outside of the scope of this research and left out in this study.

CONCLUSIONS OF MCLEAN COUNTY BRIDGE TEST

This study presented a load-rating analysis using diagnostic and proof load tests for a two-span RC slab bridge that was decommissioned and scheduled for replacement. AASHTO MBE procedures were used to obtain a modified load rating for the bridge. A summary of the main findings of this bridge study are as follows:

- Load rating using diagnostic and proof load testing showed that the bridge was capable of carrying the design loads and that no load posting should be necessary.
- The load rating improved by as much as 44% using load rating through diagnostic testing methods of the AASHTO *MBE*.
- The load rating improved by as little as 4% following load rating through proof load testing procedures of the AASHTO *MBE*. The proof test was terminated because of nonstructural damage to the roadway. Hence, a greater load rating using this test was expected.
- The proof load testing strategy was effective at demonstrating the minimum capacity for the bridge. Although, methods for decreasing the time to load the trailers using the concrete bin blocks are recommended to improve the efficiency of using this load test for load rating.

CHAPTER 5: KICKAPOO BRIDGE TEST

TESTED BRIDGE

The third bridge considered in this study was a single-span concrete slab bridge in Mattoon, Illinois. Figure 32-A presents the side view, and Figure 32-B presents the plan view and cross section. The bridge is 6.25 m (20.5 ft) long and 23.3 m (76.5 ft) wide with an aspect ratio of 3.73. The roadway is 19.5 m (64 ft) with five lanes. The sidewalk is 1.91 m (6.25 ft) and 0.64 m (25.25 in.) thick with integral concrete railings. The slab thickness is 0.32 m (12.5 in.). The droplet in the middle is 0.41 m (16 in.) thick. The concrete compressive strength in the design plans was 20.7 MPa (3,000 lbf/in^2), but core sample tests showed higher strength. In Figure 32-C, cores 1, 2, 3, and 4 are 56.4, 26.8, 48.1, and 61.7 MPa, respectively. The average strength is 48.2 MPa. The bridge reinforcement is Grade 40 #9 longitudinal bars (28.7 mm diameter) at 0.15 m (6 in.) spacing. Figure 32-B and Figure 32-C present existing damage seen during field inspection. Concrete spalling was in locations (1), (3), and (5). Spalling with reinforcement corrosion was in locations (2) and (4). Both abutments had large amounts of concrete spalling. More localized damage was in the northwest part of the bridge.

A. Bridge side view

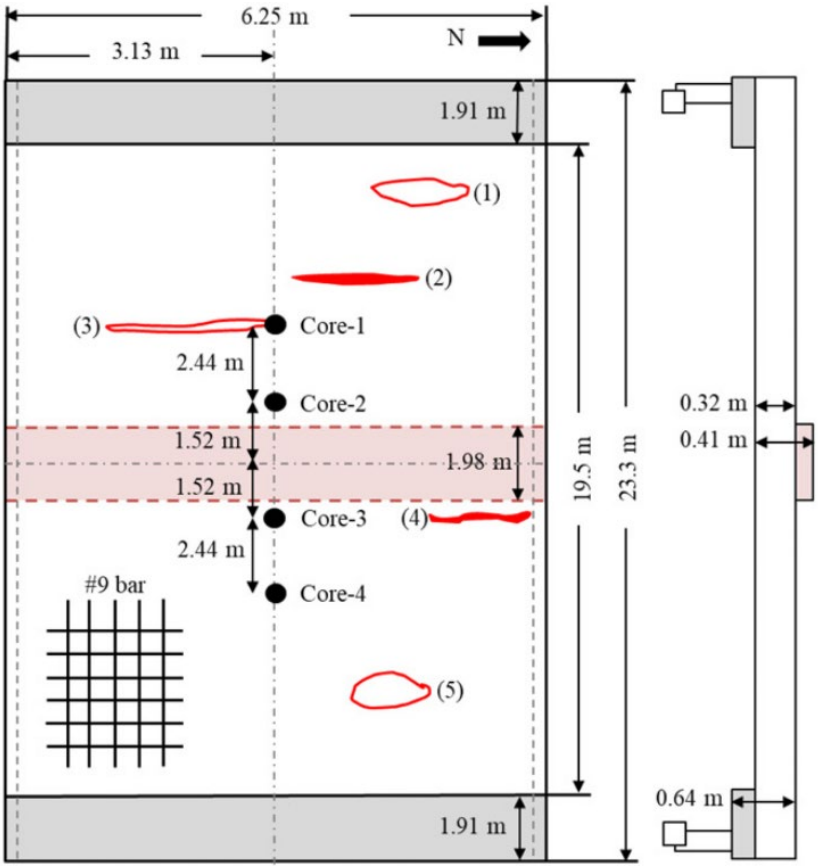

B. Plan view of the bridge with localized damage

C. Localized damage photo

Figure 32. Photo. Kickapoo bridge.

ANALYTICAL LOAD RATING OF THE BRIDGE

The bridge was constructed in 1940, before adoption of Load and Resistance Factor Design (LRFD) specifications. Therefore, the load factor rating (LFR) analytical method was used to find a rating factor of 0.675.

DIAGNOSTIC LOAD TEST PLAN

The structural testing system (STS) from Bridge Diagnostics Inc. (BDI) was used for the tests. Thirteen ST350 strain gauges measured the longitudinal strain profile of the bridge, as presented in Figure 33-A. The gauges at the ends were 1.6 m (5.25 ft) from the bridge edge, while internal gauges were 1.68

m (5.5 ft) apart. The strain range was extended to 0.46 m (18 in.) by attaching gauge extensions as presented in Figure 33-B.

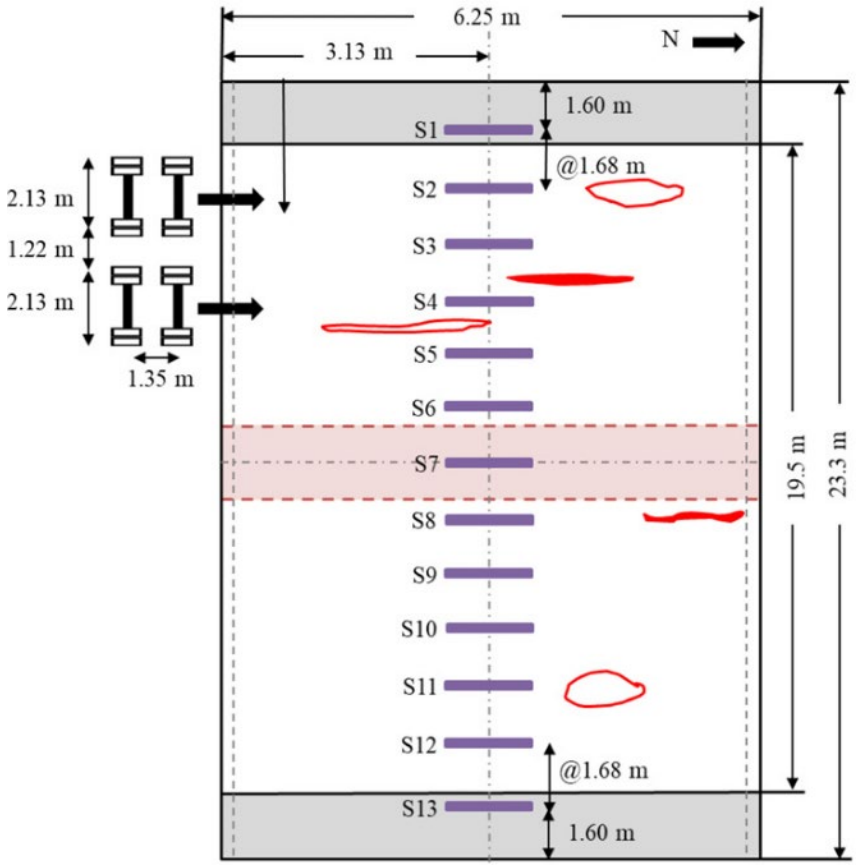

A. Instrumentation plan for the diagnostic test

B. Photograph of installed strain gauges

C. Photograph of the test trucks

Figure 33. Photo. Kickapoo diagnostic test.

The diagnostic test used two conventional IDOT dump trucks, as presented in Figure 33-C. The distance between rear axles was 1.35 m (4.42 ft). The distance between the wheels was 2.13 m (7 ft). The trucks were loaded with rocks until reaching a T/W ratio greater than 0.7 to achieve a K_b factor of 0.5. The target load was 63.6 kN (14.3 kips) per axle. The bridge span was 6.25 m (20.5 ft) so only the rear tandem axle load affected the bridge. For Truck 1, the front and rear axle tandem loads were 70.1 kN (15.75 kips) and 64.3 kN (14.45 kips), respectively. For Truck 2, the loads were 72.5 kN (16.3 kips) and 63.6 kN (14.3 kips), respectively. The diagnostic test used 10 different paths, as indicated in Table 8. For path 1, the first wheel was at 0.61 m (2 ft) from the curb and the distance between the trucks was 1.22 m (4 ft). Each path after was offset in 1.37 m (4.5 ft) increments. The trucks were driven at 2.24 m/s to load the bridge quasi-statically. Each path was repeated two times.

Table 8. Diagnostic Test Truck Locations and Maximum Strain of Kickapoo Bridge

Path	1st wheel of truck 1 from the curb (m)	1st wheel of truck 2 from the curb (m)	Max strain (με)	Strain gauge
1	0.61	3.96	28.10	S4
2	1.98	5.34	30.81	S4
3	3.35	6.71	29.99	S4
4	4.73	8.08	28.33	S5
5	6.10	9.45	25.58	S7
6	7.47	10.82	26.23	S7
7	8.84	12.20	24.86	S8
8	10.21	13.57	23.75	S10
9	11.59	14.94	34.25	S11
10	12.96	16.31	**38.79**	**S11**

Bold value refers to the maximum strain and associated sensor.

DIAGNOSTIC LOAD TEST RESULT

Figure 34 presents the critical path strain distributions. The maximum strain and corresponding strain gauge number of each path is presented in Table 8. The maximum strain was 38.79 με in strain gauge

11 (S11) during path 10. The peak strain was in the southeast part of the bridge, but the northwest part also showed significant strain (Figure 34). The K_a factor for all paths was calculated using the maximum strain ε_T in Table 8. From this, the theoretical moment was calculated. This was combined with the section modulus and modulus of elasticity to calculate ε_c by following Figure 17. The modulus of elasticity of path 10 is from concrete core sample 4, as presented in Figure 32. The section modulus uses the slab thickness. A strain limit of 132 με was calculated, which is lower than the theoretical strain, so the member behavior cannot be extrapolated to 1.33 W. The T/W value was larger than 0.7, so K_b was 0.5. By following Figure 6, K-values for all paths were obtained, and the governing value was 1.495 and an improved rating factor of 1.009 was evaluated. This is 50% higher than the analytical rating of 0.675.

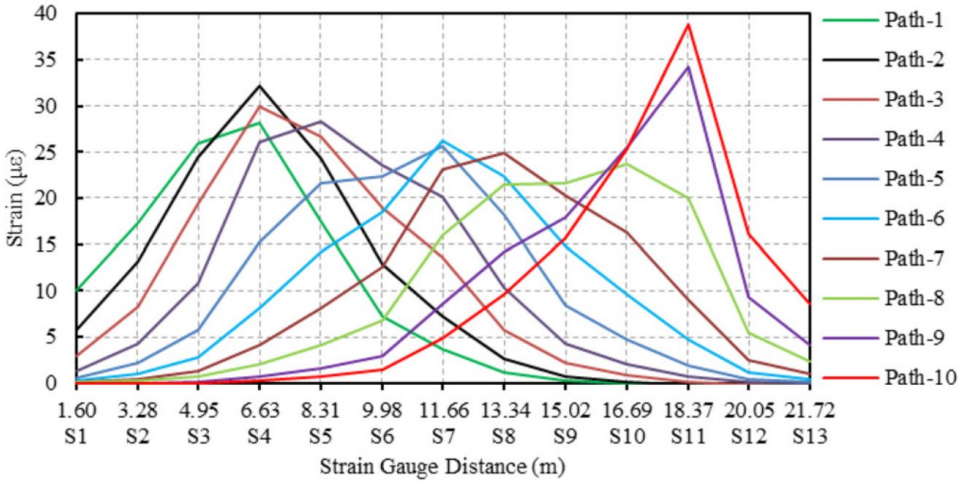

Figure 34. Graph. Strain distribution in different loading paths for double truck loading of the Kickapoo bridge.

MODIFIED LOAD RATING BASED ON STRUCTURAL EFFECTIVE WIDTH

In the structural effective width approach, the effective width per AASHTO LFR using Figure 3 can be replaced with the effective width from the load test. Researchers found it provided higher modified rating factors than the analytical approach (Saraf, 1998; Amer et al., 1999; Jones, 2011; Jáuregui et al., 2010; Lantsoght et al., 2015). Some studies considered the edge beams and sidewalks nonstructural and excluded them from the effective width calculation (Colombani & Andrawes, 2022; Freeman & Vasconcelos, 2018). Other studies that included the sidewalks found they contribute significantly to the moment distribution (Amer et al., 1999; Mabsout et al., 2004; Azizinamini et al., 1994).

The bridge in this study had large sidewalks to be considered. The moments were calculated from the measured strains and presented in Figure 34. The critical wheel load locations are presented in Figure 35-A, the strain distribution is in Figure 35-B, and the moment distribution is in Figure 35-C. The effective width is calculated by dividing the area under the curve by the maximum moment observed. The moment distribution along the cross section of the bridge is presented in Figure 35-C. The area under the curve was 53.7 kNm^2/m (39.6 $kip\text{-}ft^2/ft$). The maximum moment for the critical path was

8.58 kN-m/m (1.93 kip-ft/ft). Thus, the effective width is 6.26 m (20.53 ft), which demonstrates that a larger portion of the slab resisted the applied moment. The modified rating factor was 1.028, which is 52% higher than the analytical rating factor and 2% higher than the AASHTO MBE.

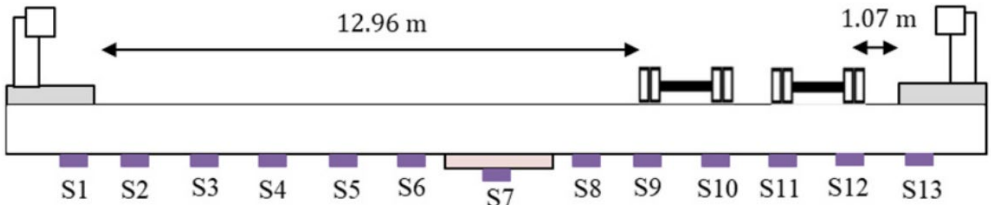

A. Wheel location of critical loading

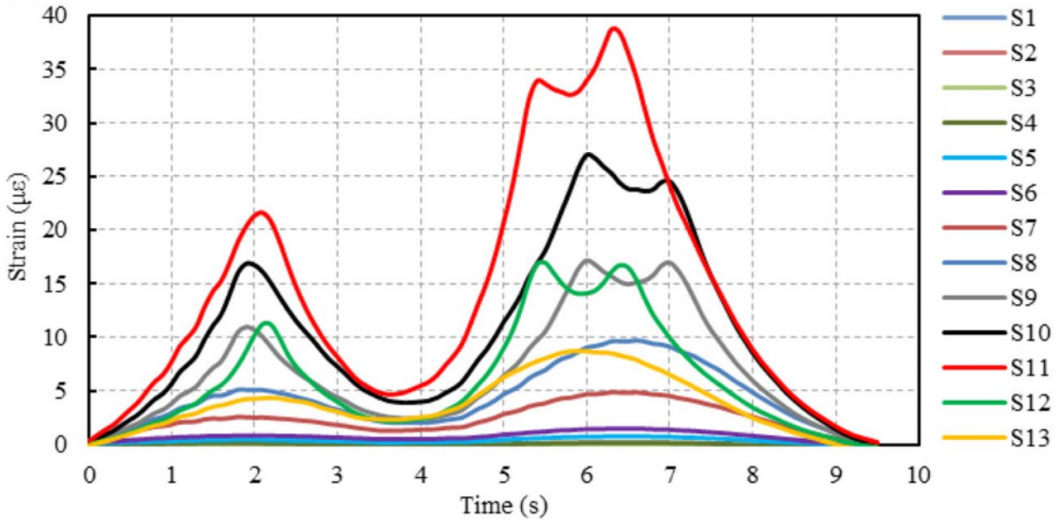

B. Strain distribution in the strain gauges

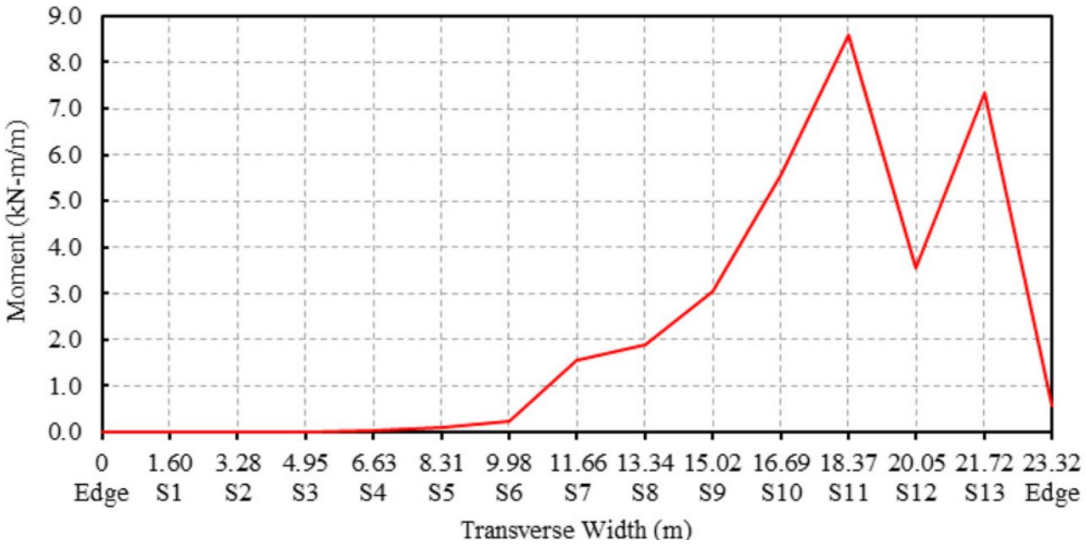

C. Moment distribution for path 10 of double truck loading

Figure 35. Graph. Double truck plots for the Kickapoo bridge.

PROOF LOAD TEST PLAN

The highest strain values in the diagnostic test were from strain gauges 4, 5, and 11 (S4, S5, and S11), as presented in Figure 34. Therefore, strain gauges were installed at only those three locations for the proof load test. Nine LVDTs, L1 through L9, were installed to measure the displacement profile in the transverse direction. The end LVDTs were placed 1.91 m (6.25 ft) from the bridge edge and the rest were installed at intervals of 2.44 m (8 ft), as presented in Figure 36-A. A photograph of the bottom is presented in Figure 36-B. Two tiltmeters (Figure 36-C) were installed near the most critical LVDTs.

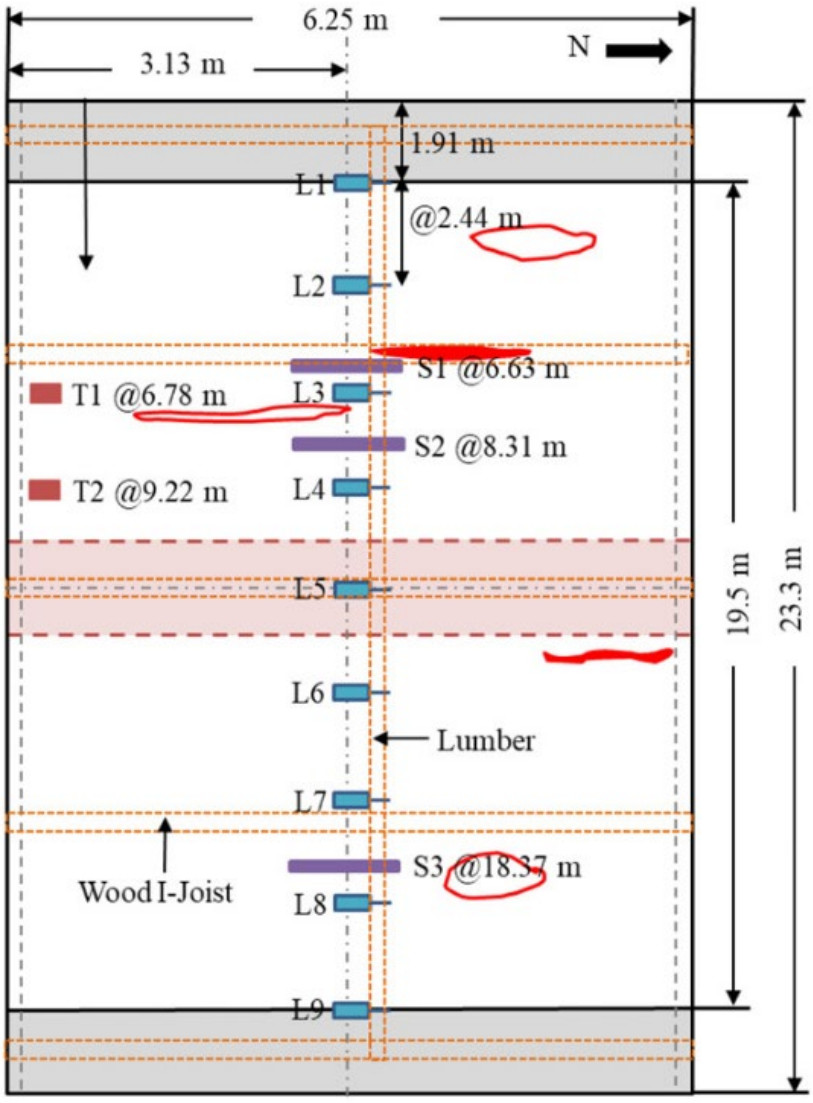

A. Instrumentation plan for the proof test

B. Wood fixture with installed LVDTs and strain gauge

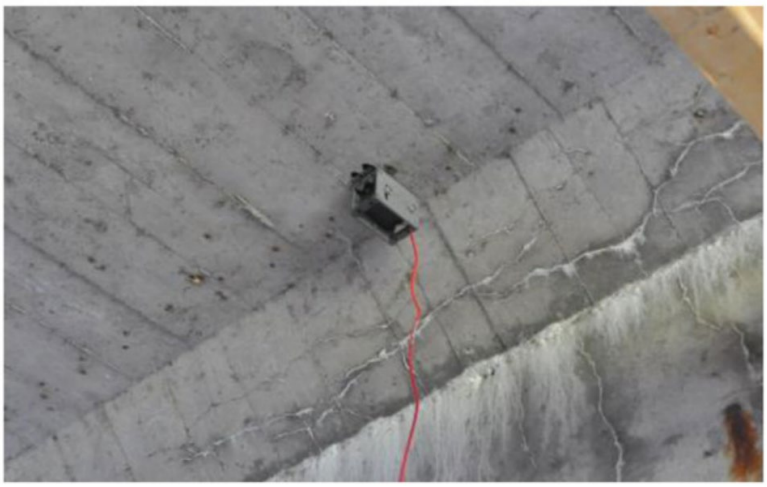

C. Tiltmeter

Figure 36. Photo. Instrumentation of Kickapoo bridge.

Only double truck loading was used in the proof test because the multilane case governed in the diagnostic test. The target moment was 2484 kN-m/m (558.4 kip-ft/ft). The magnification factor was adjusted using Figure 8 by considering the following items: the bridge was a nonredundant structure (+10%), the ADTT value is below 1,000 (−10%), and an in-depth inspection was conducted (+5%). The unfactored live load (L_R) was governed by the HS-20 truck load. For incremental loading, 16 kN (3.6 kips) concrete blocks were used, as presented in Figure 37-A. The axles were weighed using portable scales, as presented in Figure 37-B. The truck axle spacing was 1.22 m (4 ft). The bridge was 6.25 m (20.5 ft) long so only the rear axle affected the bridge. The rear axle was driven slowly over the bridge, stopped at midspan, and then driven off. In stage 1, the trailer axles produce the theoretical moments that are 26.1% of L_T based on 1D beamline analysis. The loading paths in Table 8 for the diagnostic test were followed again. The most critical paths were selected based on sensor data. The incremental loads were 48.1%, 67.6%, 81.6%, 91.2%, and 103.2% of L_T, and each stage was repeated twice. Figure 37-C presents the bridge during stage 6.

A. Loading trailer with concrete blocks

B. Weighing trailer axles

C. Loading bridge at midspan

Figure 37. Photo. Proof load testing procedure for Kickapoo bridge.

PROOF LOAD TEST RESULTS

Strain-based Result

Table 9 presents the bridge response for stage 1. The highest strain (28.43 με) was from strain gauge 3 (S3) during path 10. The highest displacement (0.358 mm) was from LVDT 3 (L3) during path 2. This finding indicates that the west side is more sensitive due to having more localized damage and, therefore, subsequent loadings were only on the west side. Path 2 (Figure 38) had the highest displacements. Figure 39 presents the strain gauge history for path 2. Both runs showed similar results for all stages. The strains in strain gauge 1 and 2 (S1 and S2) were below the cracking strain limit of 132 με in all stages. The highest strain of 103.7 με was in S1. In stage 1, there was a 30% difference between path 2 (21.79 με) and path 10 (28.43 με). The modified strain in S3 for stage 6 was 135.3 με, which is 2.5% higher than the cracking limit. This justified the decision to select paths on the west side.

Table 9. Bridge Response under Proof Load Test of Kickapoo Bridge with Maximum Strain and Displacement in Stage 1

Path	Max displacement (mm)	LVDT	Maximum strain (με)	Strain gauge
1	0.338	L3	21.01	S1
2	**0.358**	**L3**	21.79	S1
3	0.333	L3	20.78	S1
4	0.267	L3	19.50	S2
5	0.299	L4	15.97	S2
6	0.307	L5	9.37	S2
7	0.272	L6	9.11	S3
8	0.267	L7	17.01	S3
9	0.302	L7	24.67	S3
10	0.297	L8	**28.43**	**S3**

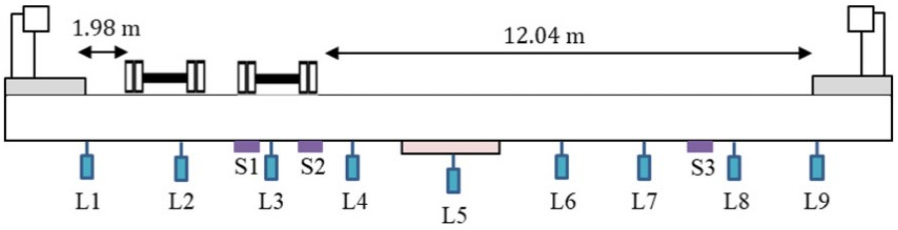

Figure 38. Illustration. Critical loading path (path 2) in the proof load test of Kickapoo bridge.

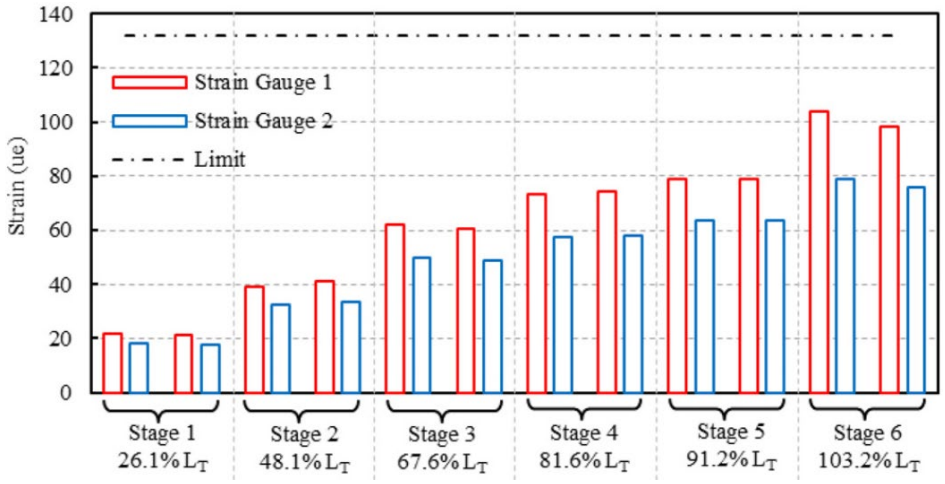

Figure 39. Graph. Strain gauge history from the proof load test of Kickapoo bridge.

Table 10. Residual Percentage in LVDTs and Tiltmeters at Loading Stages of Kickapoo bridge

Loading Stage	LVDT 3 (L3) (%)	Tiltmeter 1 (T1)	LVDT 4 (L4) (%)	Tiltmeter 2 (T2)
Stage 1	3.43	–	2.06	–
Stage 2	3.07	–	4.50	–
Stage 3	3.62	3.59%	5.47	–
Stage 4	1.06	2.17%	2.34	2.44%
Stage 5	1.99	1.64%	0.20	0.33%
Stage 6	1.05	1.07%	0.55	1.00%
Maximum	**3.62**	**3.59%**	**5.47**	**2.44%**

Bold value refers to the maximum strain and associated sensor.

Displacement-based Result

Figure 40 presents the displacement history and residual displacement for LVDT 3 and 4 (L3 and L4). LVDT 3 had the peak displacement. The residual displacement for the second run is presented in Table 10. In stage 1, both runs showed similar responses with residual displacements of 3.43% and 2.06% for LVDT 3 and 4, respectively. In the second run of stage 2, LVDT 3 showed a 7.7% increase in displacement and a residual displacement of 3.07%. There was no significant difference between the two test runs in stages 3, 4, and 5. In the second run of stage 6, there was a 4.2% reduction in the displacement of LVDT 3 and a residual displacement of 1.05%. LVDT 3 showed a cumulative residual displacement of 7.9% and LVDT 4 showed 8.4%. The second run of all loading stages showed lower displacements than the first run for both LVDTs. This indicates that the bridge is not displacing more than anticipated and can reach the target proof load. By using Figure 10 with the maximum applied live load (L_P) of 781.4 kN-m/m and k_o of 1, a modified rating factor of 1.032 is calculated. This is 53% higher than the analytical rating factor from AASHTO LFR. In Figure 41, the load-displacement responses of LVDTs are almost linear. The flexural stiffness (K) of LVDT 3 and 4 is 528.7 kN-m/mm (9,905.2 kip-ft/in) and 689.2 kN-m/mm (12,911.0 kip-ft/in), respectively. The average stiffness is 609 kN-m/mm (11,408.1 kip-ft/in). Compared to the beamline stiffness of 145 kN-m/mm (2,730.7 kip-

ft/in) in Figure 41, the stiffness differed by 76%, which corresponds to the conservative analytical rating factor.

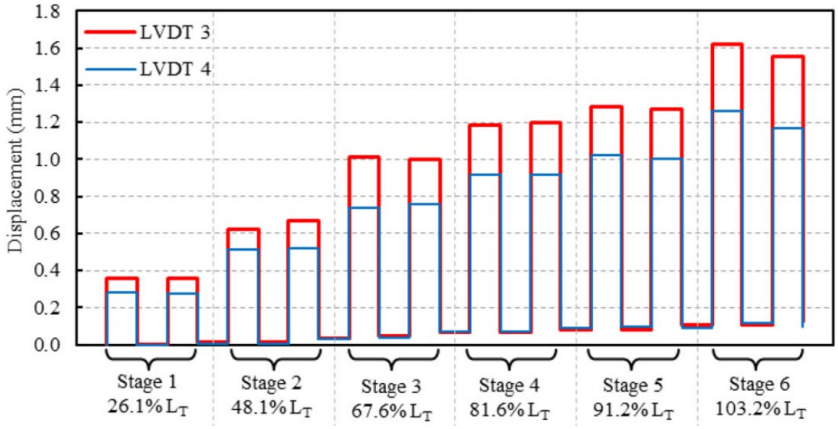

Figure 40. Graph. Load-displacement history for proof load test from LVDT 3 and LVDT 4 of Kickapoo bridge.

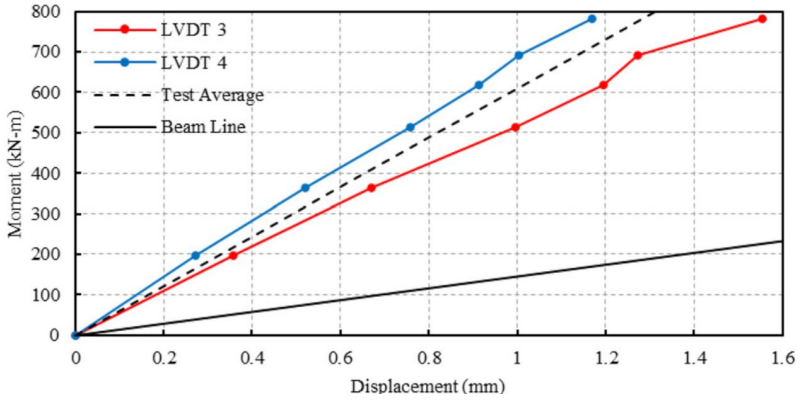

Figure 41. Graph. Flexural stiffness from the load-displacement response of LVDT 3 and LVDT 4 of Kickapoo bridge.

Rotation-based Result

Instrumenting bridges can be fast and efficient using recently developed techniques (Garnica et al., 2022). The tiltmeter is a new technique to investigate the potential of replacing LVDTs. Instrumenting LVDTs underneath the bridge is not always feasible because of water and limited accessibility. LVDTs also require a frame (Figure 36-B), which is difficult to build for longer spans. Tiltmeters need less accessibility because they are added near bridge supports. They also do not need a separate frame. Tiltmeters can measure rotation within a range of ±0.5° to ±60° (Bridge Diagnostics Inc., n.d.). Figure 36-C presents an installed tiltmeter, and Figure 36-A presents two tiltmeters mounted parallel to LVDT 3 and LVDT 4. Tiltmeter 1 was installed during stage 3 after the most critical LVDT locations were identified. Tiltmeter 2 (T2) was installed during stage 4 to check the consistency.

The load-rotation history and residual rotations from tiltmeter 1 and 2 are presented in Figure 42. The residual rotation for tiltmeter 1 and 2 for the second run is presented in Table 10. The response

from the tiltmeters was consistent with the LVDT results. In stage 3, the second run showed a 1.1% increase in rotation and a residual rotation of 3.59%, which is similar to the residual of 3.62% from LVDT 3. In stage 4, there was a 3.8% increase in rotation and a residual rotation of 2.17%. The residual in tiltmeter 1 is higher than that of LVDT 3. The residual rotation in tiltmeter 2 was 2.44%, which is similar to the residual of 2.34% from LVDT 4. In stages 5 and 6, there were no significant changes for tiltmeter 1, while tiltmeter 2 decreased by 5.2% and 4.8%. The residual rotations of tiltmeter 1 and 2 in stages 5 and 6 were close to the residual displacements of LVDT 3 and LVDT 4. The maximum residual rotation was from tiltmeter 1 and was 3.59%, which is similar to the maximum residual displacement of 3.62% from LVDT 3. If only stages 4 through 6 are compared, then the residual rotation of 2.44% from tiltmeter 2 is close to the residual displacement of 2.34% from LVDT 4. Therefore, the tiltmeters are quite promising.

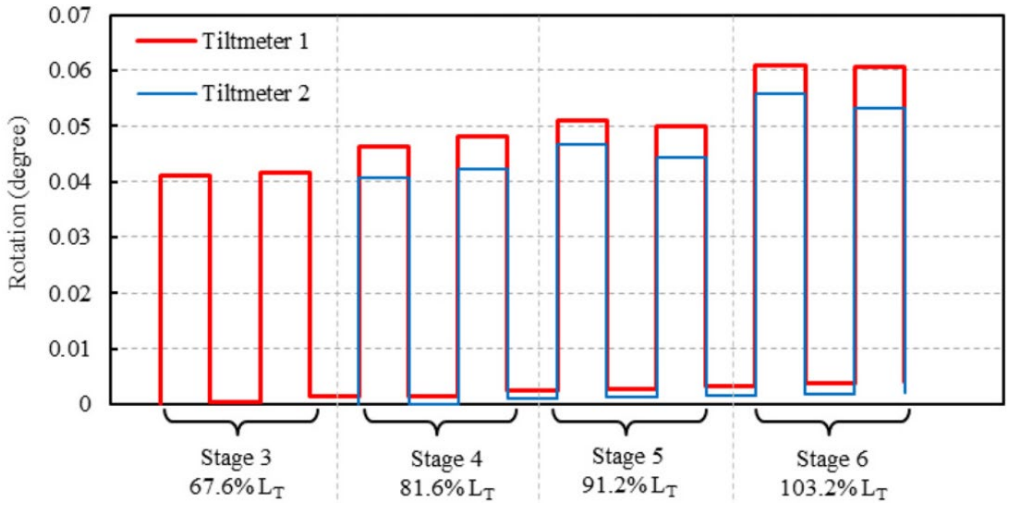

Figure 42. Graph. Load-rotation history for proof load test from tiltmeter 1 and tiltmeter 2 of Kickapoo bridge.

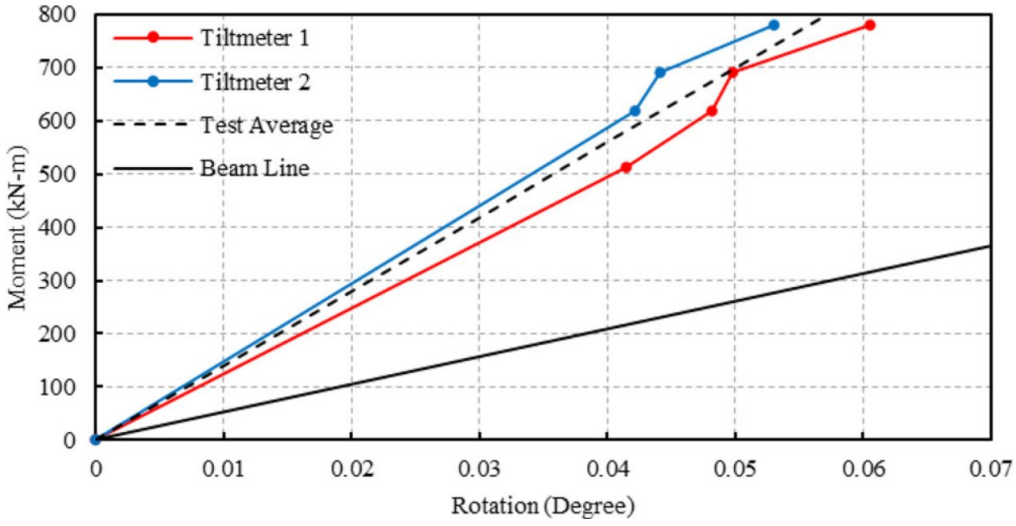

Figure 43. Graph. Rotational stiffness from the mid-span versus end rotation response of tiltmeter 1 and tiltmeter 2 of Kickapoo bridge.

ROTATIONAL STIFFNESS

The end rotational stiffness (k_θ) defines the rotational restraint at a semi-rigid beam's ends (Zhang & Xu, 2017; Xu, 2001). Bridges are assumed to be simply supported ($k_\theta = 0$) in the 1D beamline analysis but, in reality, there are end fixities due to the complicated load transfer mechanism between the bridge and supports. This study used the tiltmeter rotation results to improve the rating factor by accounting for this end rotational stiffness. Figure 43 presents the midspan moment versus the end rotation response of tiltmeters 1 and 2. The slopes of tiltmeter 1 and 2 were 12,981.2 kN-m/degree (9,574.4 kip-ft/degree) and 14,999.1 kN-m/degree (11,062.8 kip-ft/degree), respectively. The average was 13,990.1 kN-m/degree (10,318.6 kip-ft/degree). The beamline response in Figure 43 assumed no end rotational stiffness and its slope is 63%. This difference led to the conservative analytical rating factor from AASHTO LFR. The end rotational stiffness can be included as rotational springs with stiffness k_θ as presented in Figure 44. The simply supported beam with rotational spring was treated as a superposition of a simple beam with the loads and a beam with end moments. The tiltmeter rotation values from the test was used to calculate the beam end moments, and the average end rotational stiffness was 4,501.5 kN-m/ degree (3,320.1 kip-ft/degree). However, other uncertainties from material properties, localized damage, and loading conditions will also influence this stiffness.

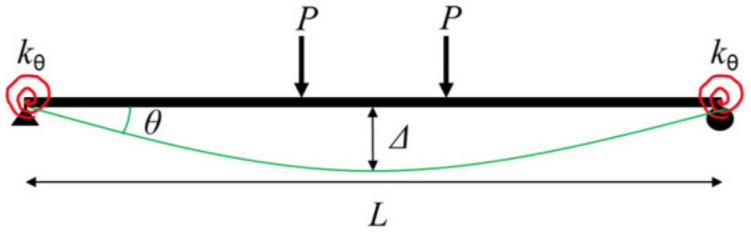

Figure 44. Illustration. Rotational stiffness of a semi-rigid beam.

Figure 45 compares a beam with rotational springs to a beam without springs. For the axle load of 309.2 kN (per axle), the displacement of a beam without springs ($k_\theta = 0$) is 5.3 mm. For the same displacement, a beam with springs (k_θ = 4501.5 kN-m/degree) can carry an axle load of 564.9 kN (per axle). This load is 83% higher than that of the beam without springs. The 1D beamline analysis was updated using the field-based rotational stiffness to find a modified load rating of 1.081. This is 60% higher than the analytical rating factor. It is 7% and 5% higher than the diagnostic and proof load test rating, respectively. Therefore, the rotational stiffness allows a more accurate representation of capacity.

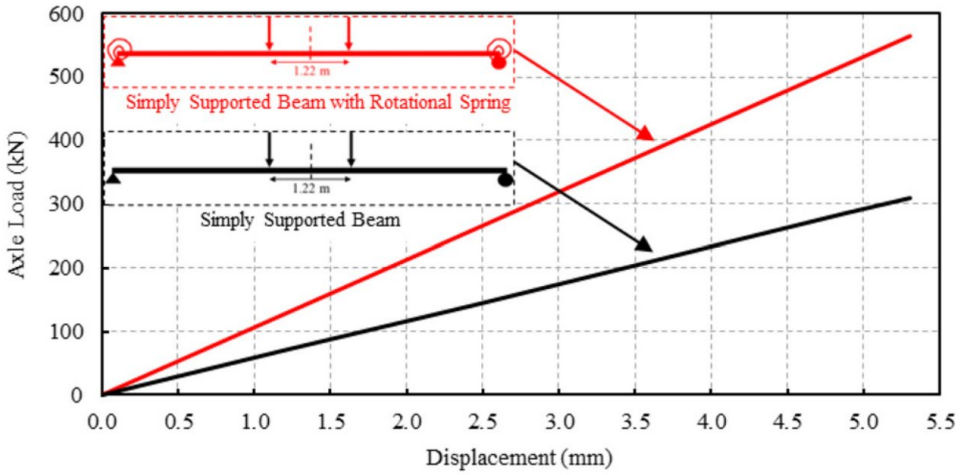

Figure 45. Graph. Comparison of calibrated load versus displacement response for a simply supported beam with rotational spring and simply supported beam.

COMPARISON OF RESULTS

Figure 46 presents a summary of the load rating results. The diagnostic test modified rating factor of 1.009 is 50% higher than the AASHTO LFR analytical rating factor. The effective width approach using the measured strains from the load test is 2% higher than the MBE approach rating factor and 52% higher than the AASHTO LFR analytical rating factor. The proof load test modified rating factor of 1.032 is 53% higher than the AASHTO LFR analytical rating factor and similar to the diagnostic test rating factor. The improved load rating is greater than 1, and no posting is needed. The AASHTO MBE approach was more conservative than the effective width approach because the diagnostic and proof load tests use only the peak strain, while the effective width approach uses all strains along the cross section. The rotational stiffness from the tiltmeter revealed that the main reason for the conservative analytical rating is the end rotational restraint and incorporation of rotational springs into the 1D beamline model increased the rating factor by 60%.

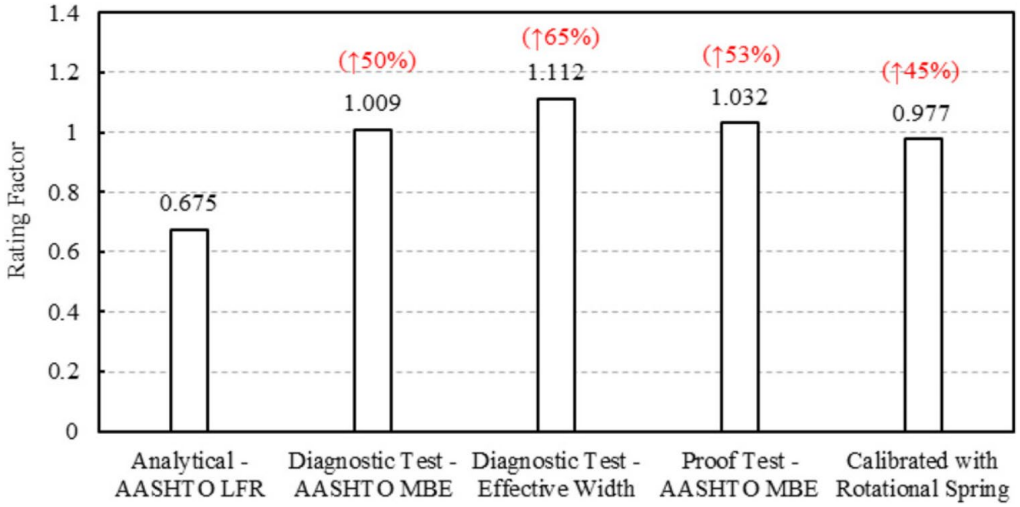

Figure 46. Graph. Rating factor comparison of Kickapoo bridge.

CONCLUSIONS

This study presented a load-rating analysis using diagnostic and proof load tests for a single-span RC slab bridge in Mattoon, Illinois. A summary of the main findings of this bridge study are as follows:

- The AASHTO MBE diagnostic and proof load tests can increase the rating factor of concrete slab bridges with localized damage.
- The AASHTO MBE diagnostic test rating factor was 50% higher than the analytical rating. The structural effective width approach rating factor was 2% higher than the MBE approach.
- The bridge carried the target proof load, which resulted in a 53% higher rating factor.
- The tiltmeters showed negligible errors in the residual response comparable to LVDTs.
- End rotational stiffnesses in the beam line model increased the load rating factor by 60%.

CHAPTER 6: COLES COUNTY BRIDGE TEST

BRIDGE DESCRIPTION

The fourth bridge considered in this study was a two-span concrete slab bridge in Coles County, Illinois. Figure 47-A presents the top of the bridge, and Figure 47-B presents the underside. The plan view and cross section are presented in Figure 47-C. The bridge is 17.9 m (58.7 ft) long and 11.1 m (36.3 ft) wide. The bridge has a clear roadway of 9.1 m (30 ft) and 0.97 m (3.2 ft) sidewalks with railings. The slab thickness is 0.36 m (14 in.), and the sidewalk curb thickness is 0.66 m (26 in.). The skew angle of the bridge is 55°. The reinforcement is #8 bars at 152 mm (6 in.) spacing. Cracks, spalling, and honeycombs were noticed during field inspection. Figure 47-C presents the plan view of the bridge with areas of damage labeled. Figure 47-D presents close-up images of the localized damage.

A. Top of bridge

B. Underneath the bridge

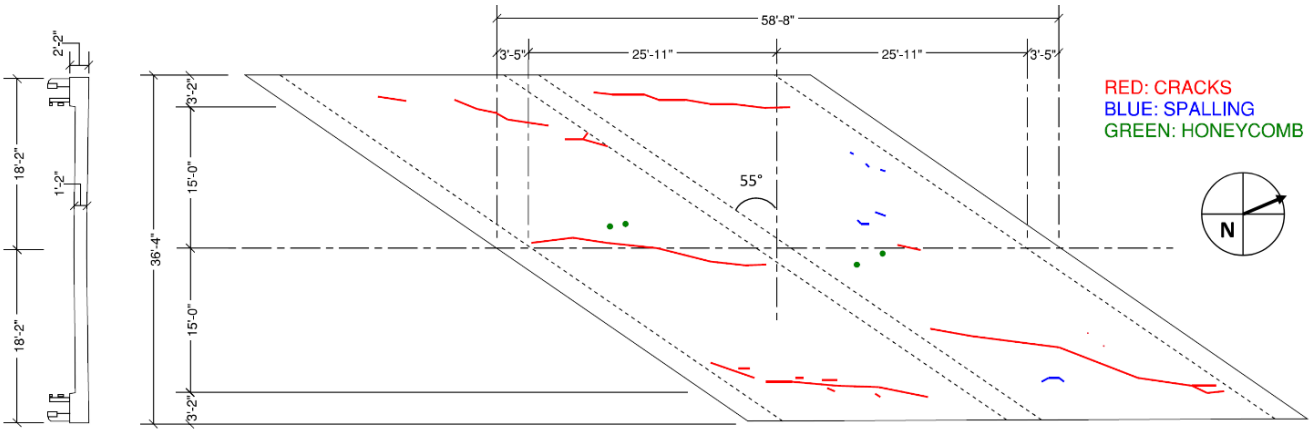

C. Bridge plan

D. Localized damage

Figure 47. Photo. Coles County bridge.

ANALYTICAL LOAD-RATING RESULTS

The bridge was evaluated under single-truck and double-truck loading to determine the greatest load effects. The locations of the two trucks in the double-truck loading condition were offset to account for the skew angle, and the rating factor was 0.688.

DIAGNOSTIC TEST SENSOR PLAN AND LOADING PLAN

The STS system used in previous tests was used again for this bridge. A total of 12 strain gauges were mounted to the bridge bottom, as presented in Figure 48-A. It was not clear which span would be more critical, so initially, each span was equipped with 6 evenly spaced strain gauges.

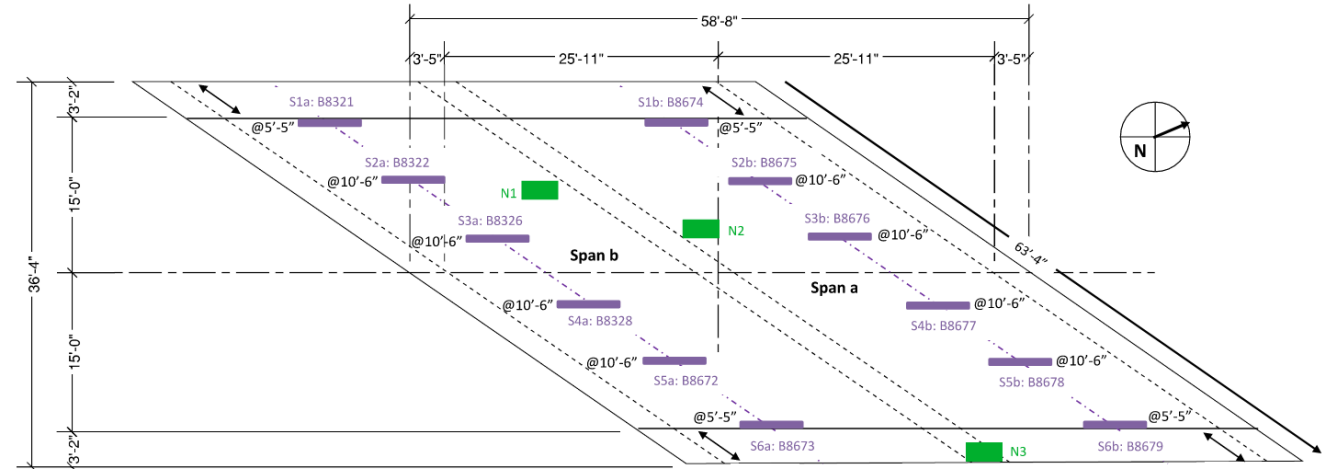

A. Phase 1 layout

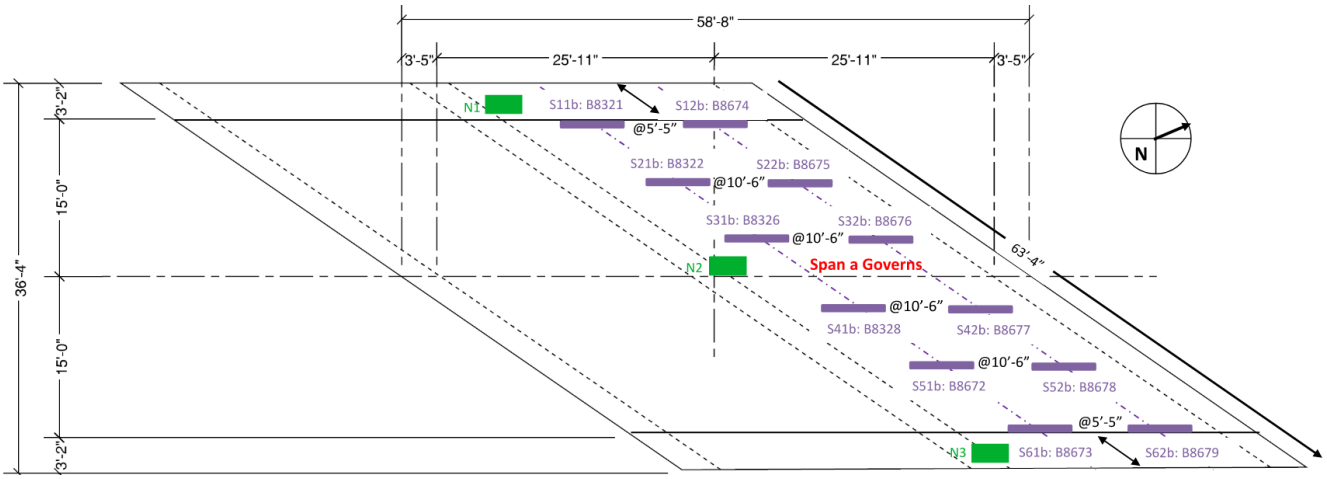

B. Phase 2 layout

Figure 48. Illustration. Instrumentation plan for Coles County bridge.

The bridge was loaded simultaneously with two IDOT trucks. Figure 49 presents the axle spacings. The trucks were loaded to reach a K_b factor of 0.5 by having the T/W ratio be greater than 0.7.

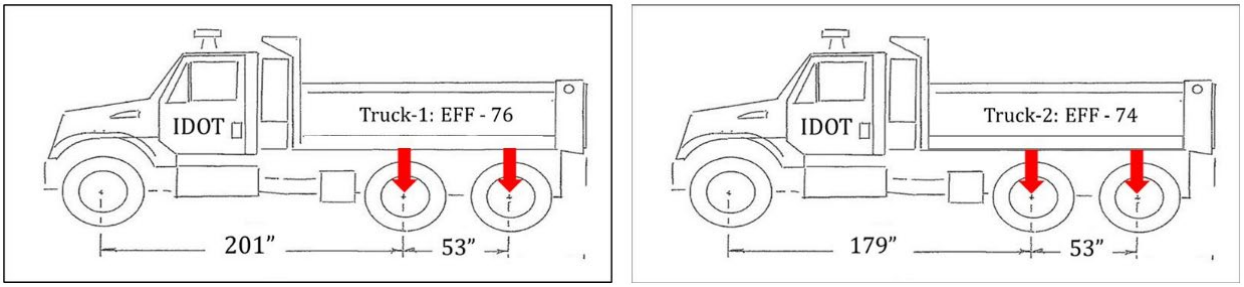

Figure 49. Illustration. IDOT trucks for Coles County bridge test.

The diagnostic test was divided into two phases. During the first phase, the strain gauge readings from both spans were compared to determine which span was more critical. Once the span with the highest strain was determined, all strain gauges were moved to that span for the second phase. The loading was then repeated twice. Table 11 summarizes the maximum strains and their respective strain gauges.

Table 11. Diagnostic Test Maximum Strains for Coles County Bridge

	Phase 1		Phase 2			
	Max Strain (με)	Strain Gauge	Max Strain (με)	Strain Gauge	Max Strain (με)	Strain Gauge
	Span a (Average	@12'8")	Span a (Pin-Pin	@11')	Span a (Fix-Fix	@14'5")
Path 1	10.98	B8676	8.96	B8677	8.52	B8328
Path 2	12.24	B8675	9.21	B8675	8.82	B8322
Path 3	8.68	B8676	10.61	B8678	8.02	B8672
	Span b (Average	@12'8")				
Path 1	9.56	B8328				
Path 2	8.77	B8328				
Path 3	9.54	B8672				

DIAGNOSTIC TEST LOAD-RATING RESULTS

The cracking moment was calculated, and the member behavior could not be extrapolated to 1.33 W. Figure 50-A presents the strain distribution, and Figure 50-B presents the corresponding moment distribution. The maximum strain was 12.24 με from path 2 of Phase 1. From this, a K_a factor of 6.23 was calculated. The T/W ratio was larger than 0.7, so the K_b factor is 0.5. By using Figure 6, a K-factor of 4.11 was calculated and the modified rating factor was 2.829. The structural effective width approach introduced for the Kickapoo bridge was also used for this study, and the rating factor was 0.726.

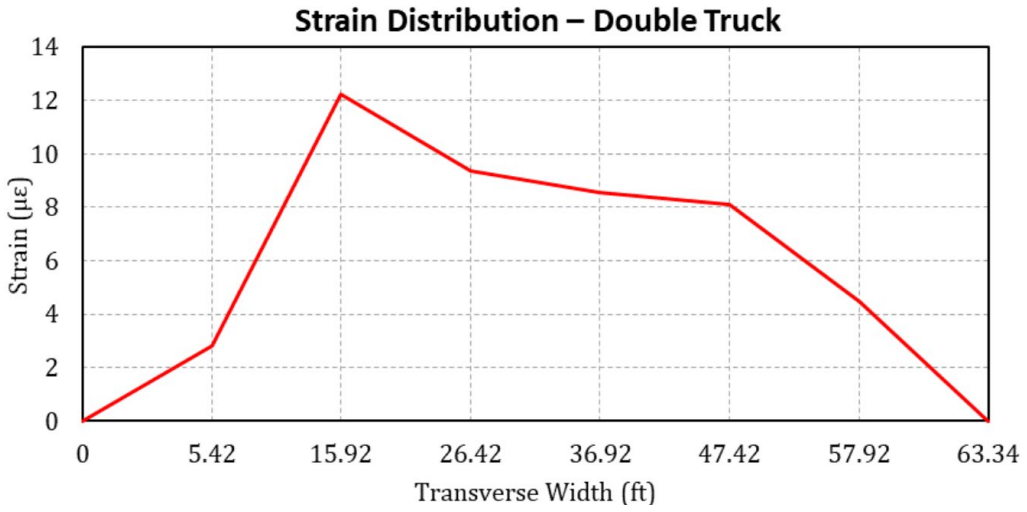

A. Strain distribution

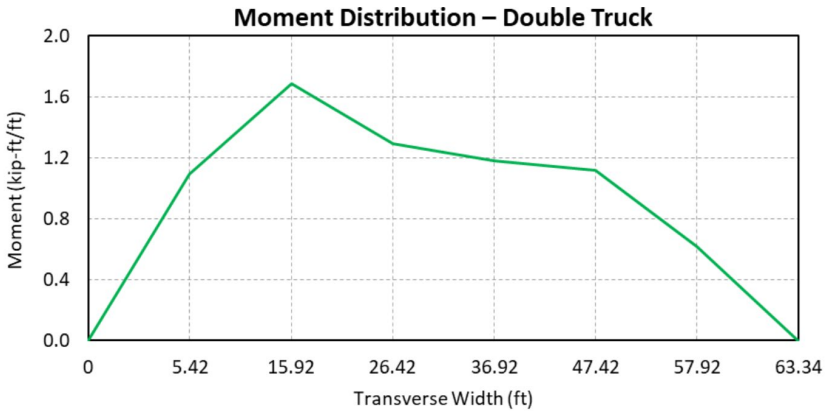

B. Moment distribution

Figure 50. Graph. Plots along transverse width of Coles County bridge.

PROOF TEST SENSOR PLAN AND LOADING PLAN

The diagnostic test indicated the northmost span as the most critical, so only that span was instrumented for the proof test. A total of 6 LVDTs, 7 strain gauges, and 7 tiltmeters were attached to the bottom of the bridge, as presented in Figure 51-A. Three of the strain gauges were installed above the bridge between the two spans to study the positive moments, as seen in Figure 51-B. The remaining four strain gauges were placed underneath the slab at the midspan. Four LVDTs were placed near the bottom strain gauges and the other two were placed 0.97 m (3.2 ft) away from the edges. Figure 51-C presents a close-up of these instruments. The tiltmeters were placed near the abutments, with three on the south side and four on the north side. Figure 51-D presents a picture of a tiltmeter.

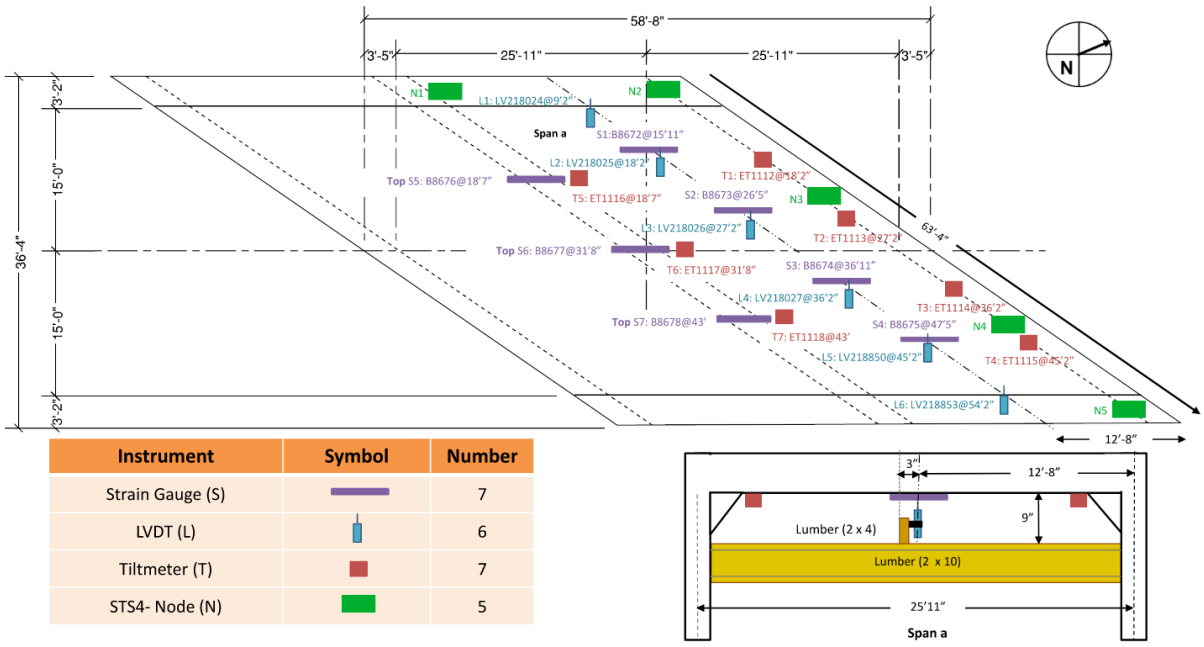

Instrument	Symbol	Number
Strain Gauge (S)		7
LVDT (L)		6
Tiltmeter (T)		7
STS4- Node (N)		5

A. Instrumentation plan

B. Strain gauges above the slab

C. LVDT and strain gauge underneath the slab

D. Tiltmeter

Figure 51. Photo. Proof test instrumentation of Coles County bridge.

A positive target proof moment of 2,512 kN-m/m (564.8 kip-ft/ft) and negative target proof moment of 2,483 kN-m/m (558.1 kip-ft/ft) was calculated. The magnification factor was adjusted by accounting for an ADTT value below 1,000 (−10%) and an in-depth inspection (+5%) using Figure 8. The loading was amplified by adding 16 kN (3.6 kips) concrete bin blocks and checking the axle weights. The incremental loads on the bridge were 44.4%, 62.3%, 79.7%, 90.4% and 101.3% of L_T. Each loading stage was repeated twice. Table 12 summarizes the moments for different stages.

Table 12. Positive Moment for All Stages of Coles County Bridge

Stage	%	Positive Moment (kip-ft)	Truck Per Axle (kip)	Trailer Per Axle (kip)
1	44.4	250.8	**17.2**	–
2	62.3	351.8	**17.2**	16.3
3	79.7	450.1	**17.2**	23.4
4	90.4	510.4	**17.2**	28.0
5	101.3	572.3	**17.2**	32.4

PROOF TEST LOAD-RATING RESULTS

The previously used spreadsheet made in Microsoft Excel was reused to evaluate the linearity of the bridge response during the test. The results recorded were viewed in the STS-LIVE software and processed in Excel after each run. For each LVDT, a load-displacement plot and a displacement history plot were created (Figure 52). For each strain gauge, a load-strain plot and a strain history plot were created (Figure 53). For each tiltmeter, a load-rotation plot and a rotation history plot were created (Figure 54). The history plots track the residuals from each stage.

Because the effect of the end fixity could not be determined, the load rating was calculated twice. The first value assumed a pin-pin end condition, which gave an RF of 0.706. The second assumed a fix-fix end condition, which gave an RF of 0.704. These two values were averaged to obtain a modified RF equal to 0.705, which is a 2% improvement from the analytical results.

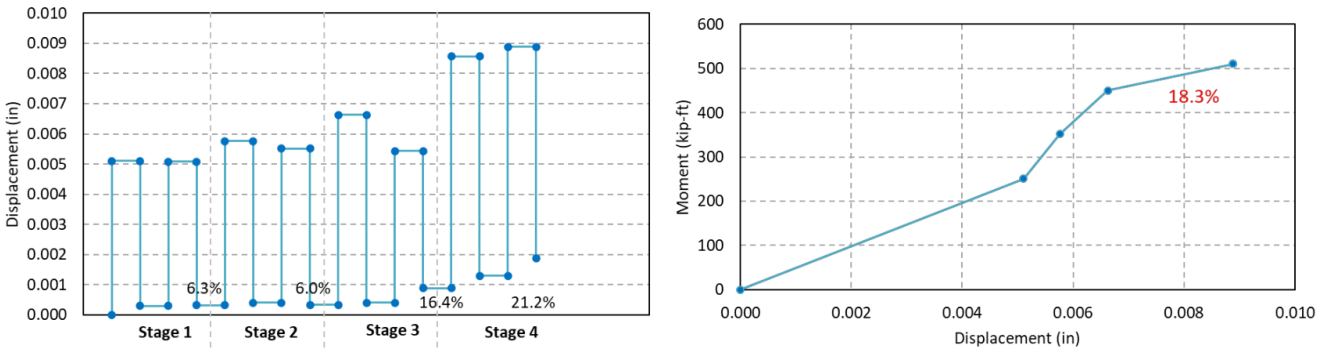

Figure 52. Graph. Displacement plots of Coles County bridge.

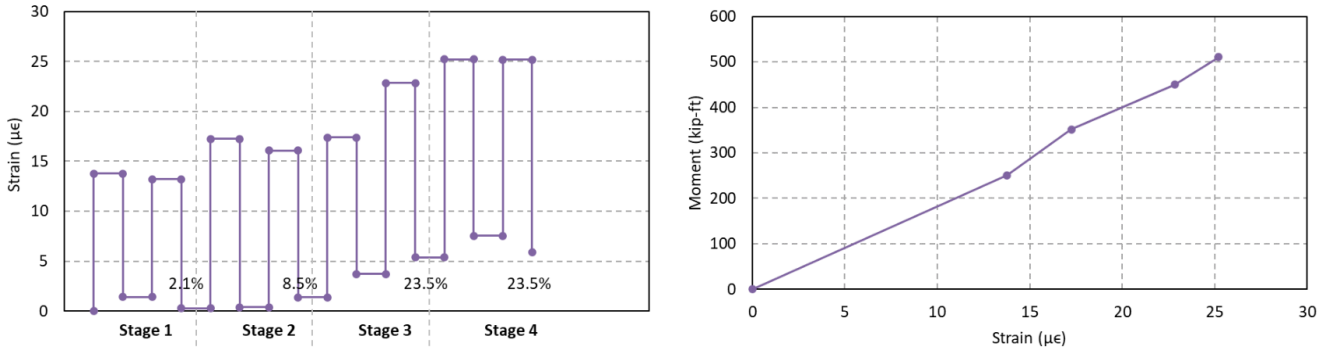

Figure 53. Graph. Strain plots of Coles County bridge.

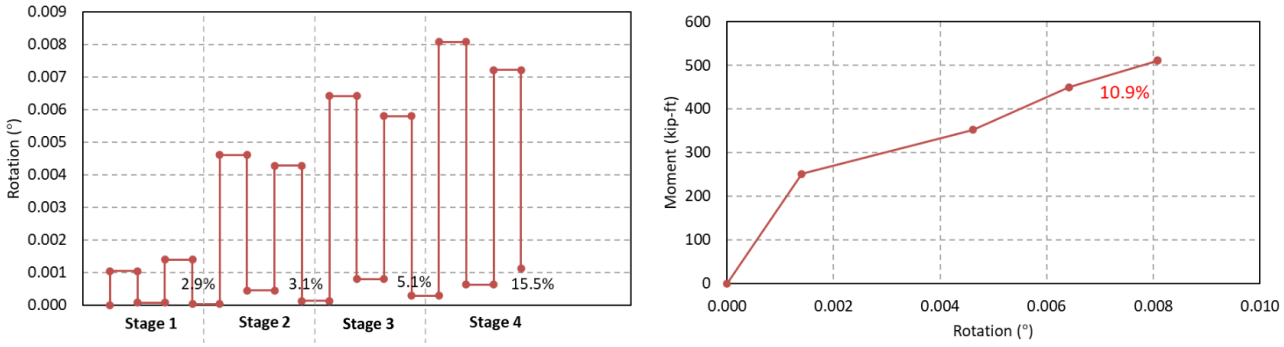

Figure 54. Graph. Rotation plots of Coles County bridge.

RESULTS AND DISCUSSION OF COLES COUNTY BRIDGE TEST

Figure 55 presents a summary of the load-rating results. The diagnostic test provided a modified rating factor of 2.829, which is 312% higher than the AASHTO LFR analytical rating factor. The effective width approach showed an improvement of 6% over the AASHTO LFR analytical rating. The proof-load test rating (average of pin-pin and fix-fix) was 2% higher than the AASHTO LFR analytical rating factor. The proof-load test provided a more realistic rating factor than the diagnostic MBE test.

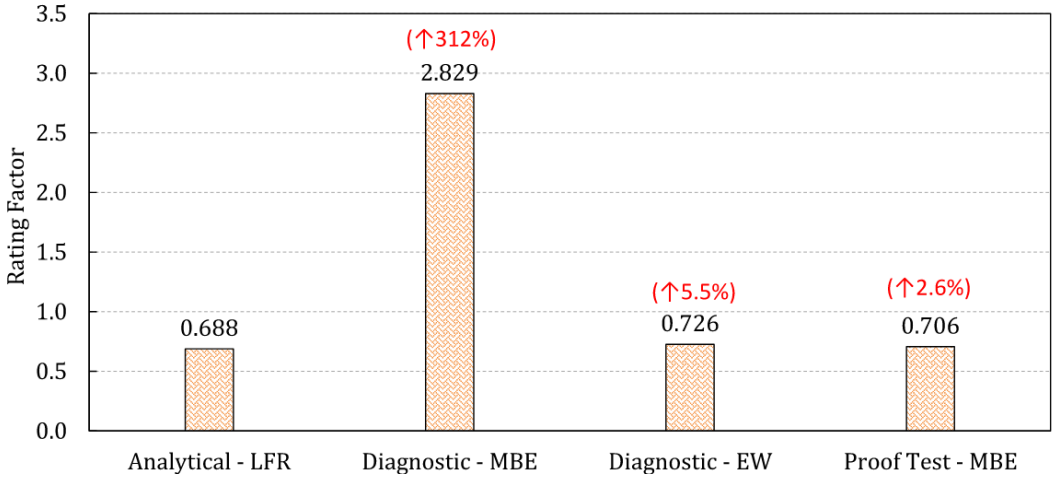

Figure 55. Graph. Load-rating summary of Coles County bridge.

CONCLUSIONS OF COLES COUNTY BRIDGE TEST

The following are the main outcomes of the study:

- The K-factor in the diagnostic load rating is not suitable for highly skewed concrete slab bridges.
- Due to the skew, the actual strain gauge orientation might be different, which is reflected in the MBE load rating.
- The rating factor using the effective structural width method is 5.5% higher than that of the analytical rating.
- The proof load test provided a more realistic rating factor than the diagnostic test.
- The proof load test rating (average of pinned-pinned and fixed-fixed) is 2.6% higher than that of the analytical rating factor.
- “Posting” will be required for this bridge based on the load test.

CHAPTER 7: 0740013 BRIDGE TEST

BRIDGE DESCRIPTION

The fifth bridge considered in this study was a single-span concrete slab bridge in Piatt County, Illinois. The coordinates of the bridge are 40.05426217, -88.745333. Figure 56 presents the plan view and cross section. The bridge is 9.8 m (32 ft) long and 12.2 m (40 ft) wide. The bridge has sidewalks on both sides with integral concrete railings. The slab thickness is 0.6 m (22.3 in.), and the sidewalk curb thickness is 0.7 m (26.3 in.). The reinforcement was staggered #9 bars. Figure 57-A and Figure 57-B present the top and bottom of the bridge, respectively. Cracks and spalling of the bottom slab were noticed during field inspection. Figure 57-C presents close-up images of the localized damage.

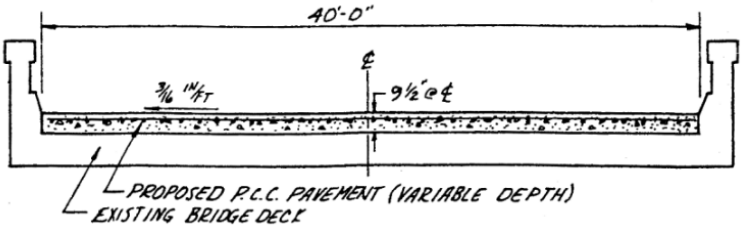

A. Elevation view

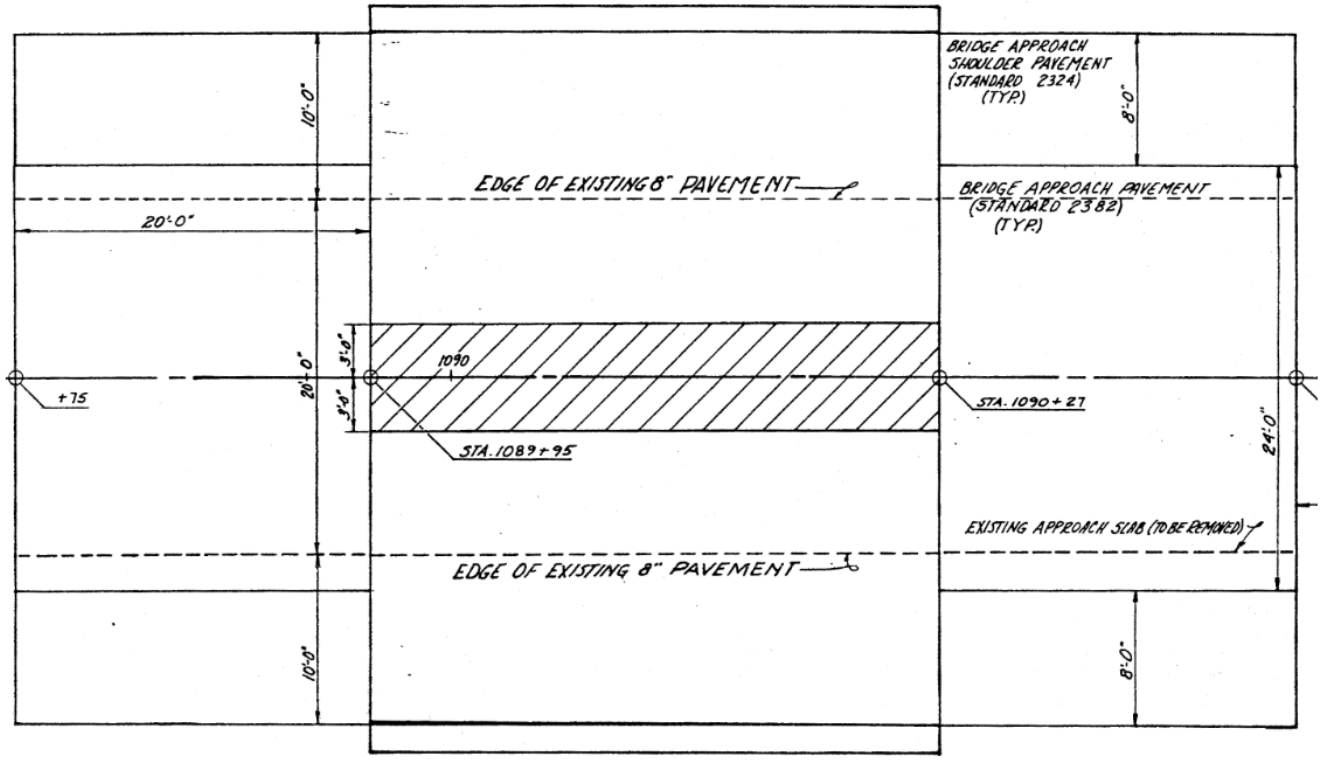

B. Plan view

Figure 56. Illustration. Original plans of 0740013 bridge.

A. Top of bridge

B. Underneath bridge

C. Close-up of damage

Figure 57. Photo. 0740013 bridge.

ANALYTICAL LOAD-RATING RESULTS

Around this time, the IDOT team was trained on how to prepare for and conduct the tests, so the IDOT team conducted the analysis. The rating factor was 1.064.

DIAGNOSTIC TEST SENSOR PLAN AND LOADING PLAN

The IDOT team primarily carried out the diagnostic test. They planned the instrumentation layout and operated the STS4 system. A total of 9 strain gauges were mounted to the bridge bottom, as presented in Figure 58.

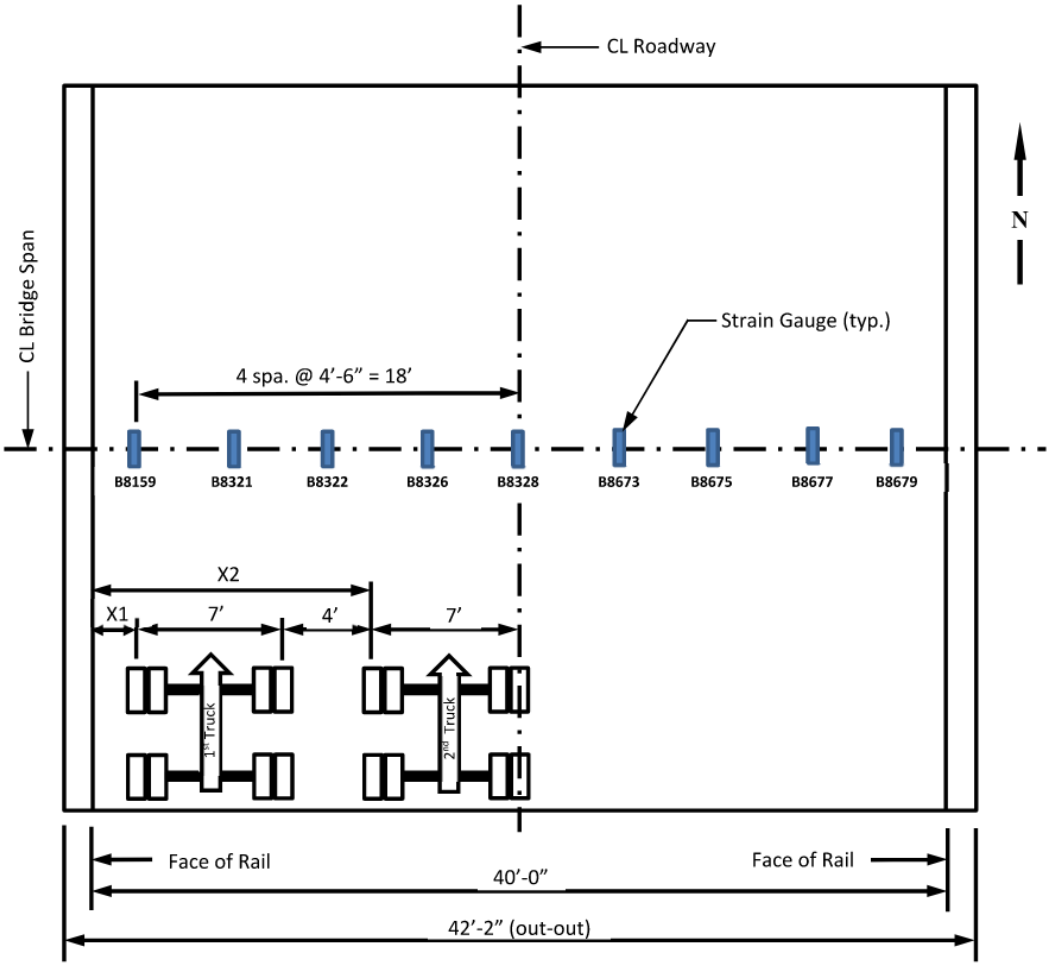

Figure 58. Illustration. Instrumentation plan of 0740013 bridge.

The bridge was loaded simultaneously with two IDOT trucks. The wheels were 2.13 m apart, and the trucks were 1.22 m apart. The trucks were loaded to reach a K_b factor of 0.5 by having the T/W ratio be greater than 0.7. IDOT determined the target axle load to be 16 kip. IDOT documented the peak strains and corresponding strain gauges, presented in Table 13.

Table 13. Diagnostic Strain Data for 0740013 Bridge

Path	1 Truck		2 Trucks	
	Max Strain (με)	Strain Gauge	Max Strain (με)	Strain Gauge
1	10.07	B8159	15.23	B8159
2	7.45	B8321	13.41	B8328
3	7.44	B8328	15.41	B8328
4	9.18	B8328	18.81	B8677
5	7.66	B8328	***22.83***	***B8677***
6	11.75	B8677		
7	14.20	B8677		
8	***14.45***	***B8677***		

DIAGNOSTIC TEST LOAD-RATING RESULTS

IDOT then used the data to calculate the load-rating factors. The diagnostic test load rating for a single truck is 3.62 and the load rating for two trucks is 2.70. For the effective width method, the rating factors for a single truck and two trucks are 1.18 and 0.74, respectively.

PROOF TEST SENSOR PLAN AND LOADING PLAN

By using the data from the diagnostic test, IDOT determined the instrumentation and loading for the proof test. A total of 9 LVDTs and 3 strain gauges were attached to the bottom of the bridge. Figure 59 presents the instrumentation plan, and Figure 60 displays a close-up of these instruments.

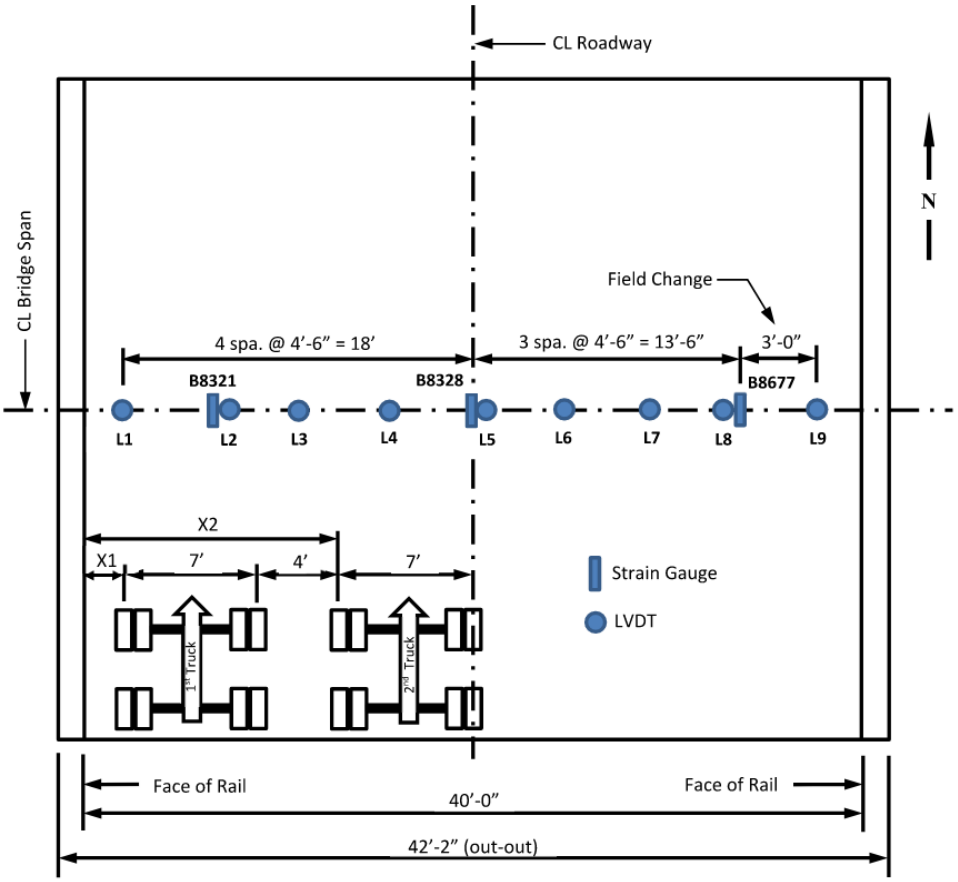

Figure 59. Illustration. Instrumentation plan of 0740013 bridge.

Figure 60. Photo. Photo of instruments under 0740013 bridge.

Table 14 presents the target loads for each stage. For the incremental loading on the bridge, concrete blocks were added to the trucks. Two different weights can be seen in Figure 61. The bridge was able to carry 100% of the target load without any issues. IDOT completed the analysis and results internally.

Table 14. Proof Load Stages for 0740013 Bridge

Stage	%	Weight Per Axle (kip)
1	25%	9.4
2	50%	18.8
3	65%	24.4
4	80%	30.1
5	90%	33.8
6	100%	37.6

A. First stage

B. Final stage

Figure 61. Photo. Photographs of testing at different stages of 0740013 bridge test.

CHAPTER 8: 0740016 BRIDGE TEST

BRIDGE DESCRIPTION

The sixth bridge considered in this study was a single-span concrete slab bridge in Piatt County, Illinois. The coordinates of the bridge are 40.05426217, -88.74515456. Figure 62 presents the plan view and cross section. The bridge has a skew of 30°. The bridge is 7.8 m (25.5 ft) long and 12.2 m (40 ft) wide. The bridge has sidewalks on both sides with integral concrete railings. The slab thickness is 0.4 m (16.5 in.), and the sidewalk curb thickness is 0.6 m (22 in.). The reinforcement is #8 bars. Figure 63-A and Figure 63-B present the top and bottom of the bridge, respectively. Cracks and spalling of the bottom slab were noticed during field inspection. Figure 63-C presents close-up images of the localized damage.

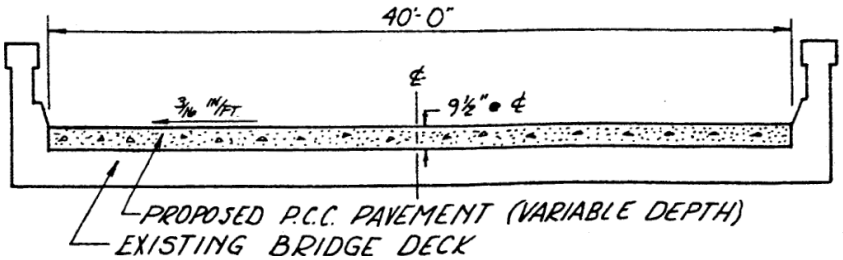

A. Elevation view

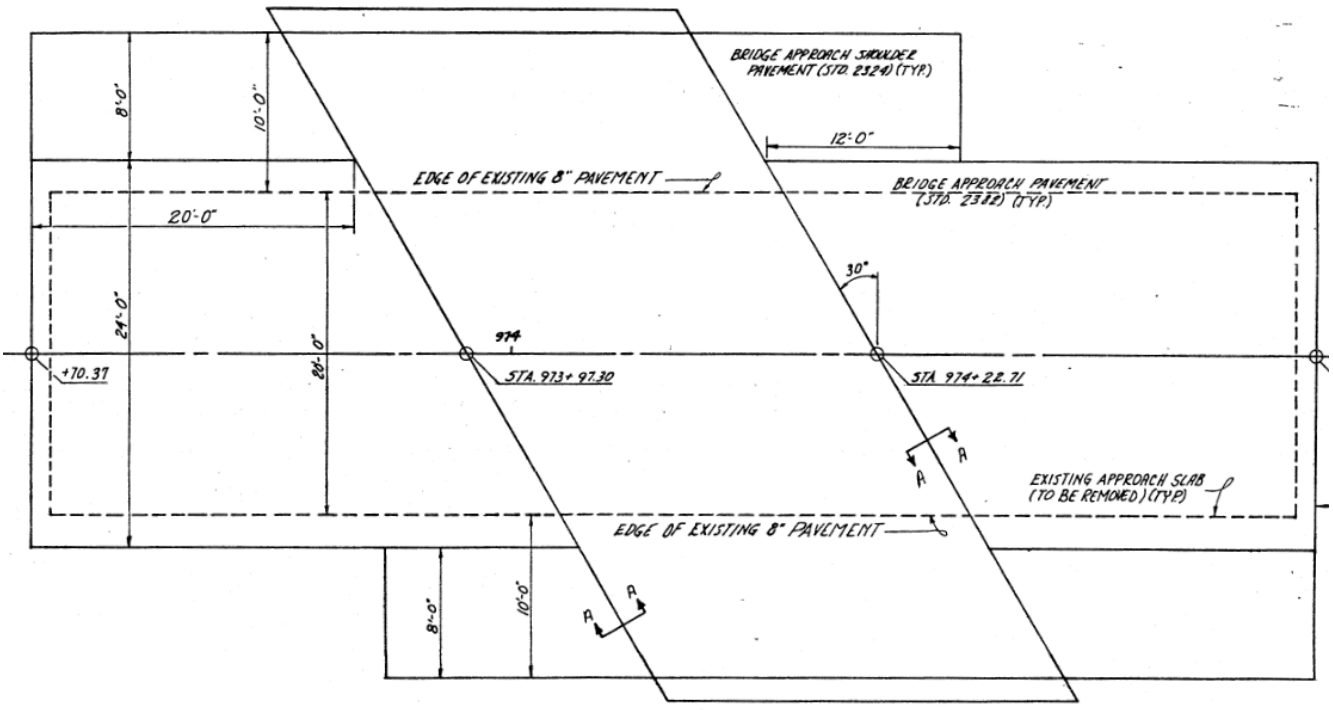

B. Plan view

Figure 62. Illustration. Original plans for 0740016 bridge.

A. Top of bridge

B. Underneath bridge

C. Close-up of damage

Figure 63. Photo. 0740016 bridge.

ANALYTICAL LOAD-RATING RESULTS

By this point, IDOT was in charge of the full process. The IDOT team conducted the analysis, and they found the rating factor to be 0.96.

DIAGNOSTIC TEST SENSOR PLAN AND LOADING PLAN

The IDOT team carried out the diagnostic test. They planned the instrumentation layout and operated the STS4 system. A total of 9 strain gauges were mounted to the bridge bottom, as presented in Figure 64. IDOT documented the peak strains and corresponding strain gauges, presented in Table 15.

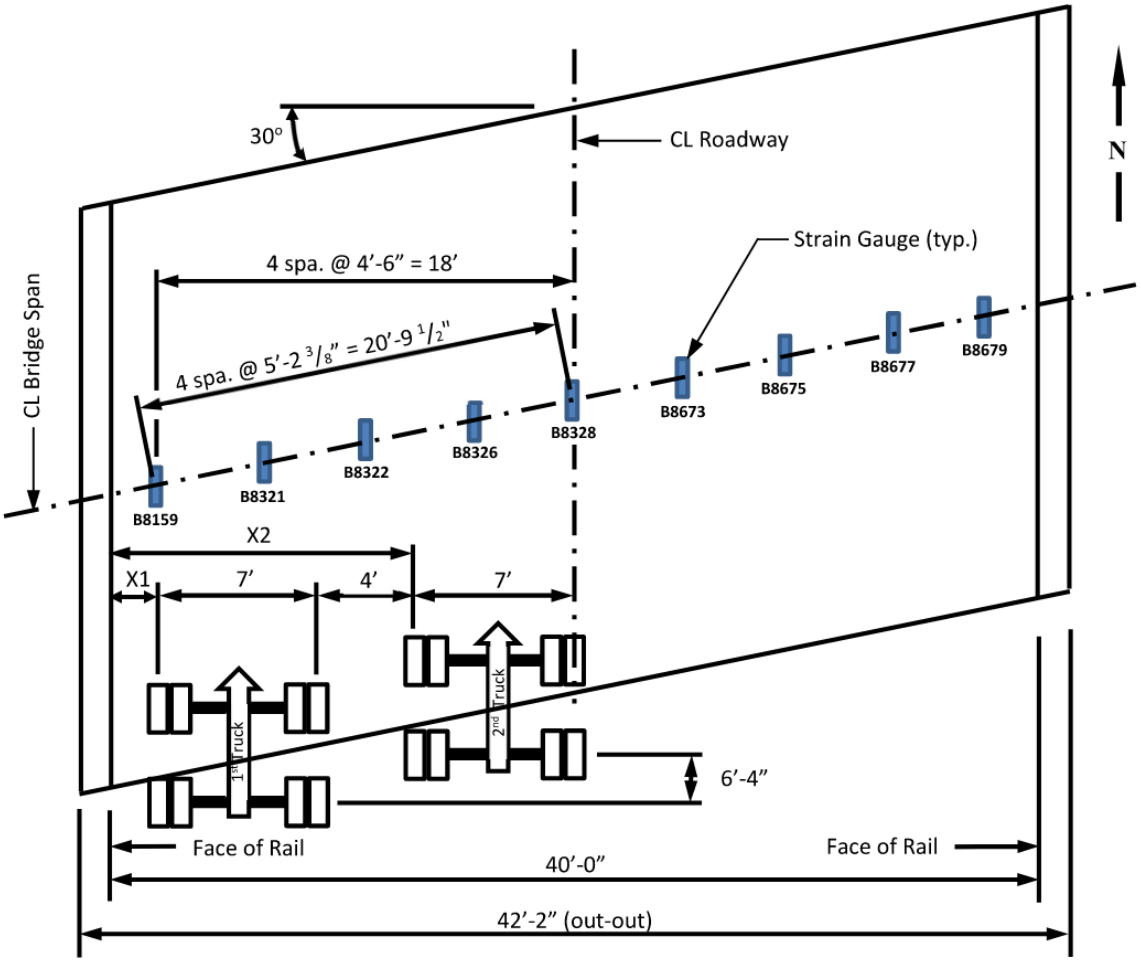

Figure 64. Illustration. Instrumentation plan of 0740016 bridge.

The bridge was loaded simultaneously with two IDOT trucks. The wheels were 2.13 m apart, and the trucks were 1.22 m apart. The trucks were loaded to reach a K_b factor of 0.5 by having the T/W ratio be greater than 0.7. IDOT determined the target axle load to be 14 kip. IDOT documented the peak strains and corresponding strain gauges, presented in Table 15.

Table 15. Diagnostic Strain Data for 0740016 Bridge

Path	1 Truck		2 Trucks	
	Max Strain (με)	Strain Gauge	Max Strain (με)	Strain Gauge
1	14.29	B8321	***18.94***	***B8321***
2	***15.55***	***B8321***	17.43	B8321
3	12.32	B8326	15.33	B8326
4	11.35	B8326	12.87	B8326
5	8.44	B8328	9.89	B8673
6	8.44	B8675		
7	7.96	B8675		
8	7.99	B8679		

DIAGNOSTIC TEST LOAD-RATING RESULTS

IDOT documented the maximum strains from the test and used them to calculate the rating factor. The load rating for a single truck is 4.15, and the load rating for two trucks is 3.66. For the effective width method, the rating factors for a single truck and two trucks are 1.13 and 0.77, respectively.

PROOF TEST SENSOR PLAN AND LOADING PLAN

By using the data from the diagnostic test, IDOT determined the instrumentation and loading for the proof test. A total of 9 LVDTs and 3 strain gauges were attached to the bottom of the bridge. Figure 65 presents the instrumentation plan, and Figure 66 presents a close-up of these instruments.

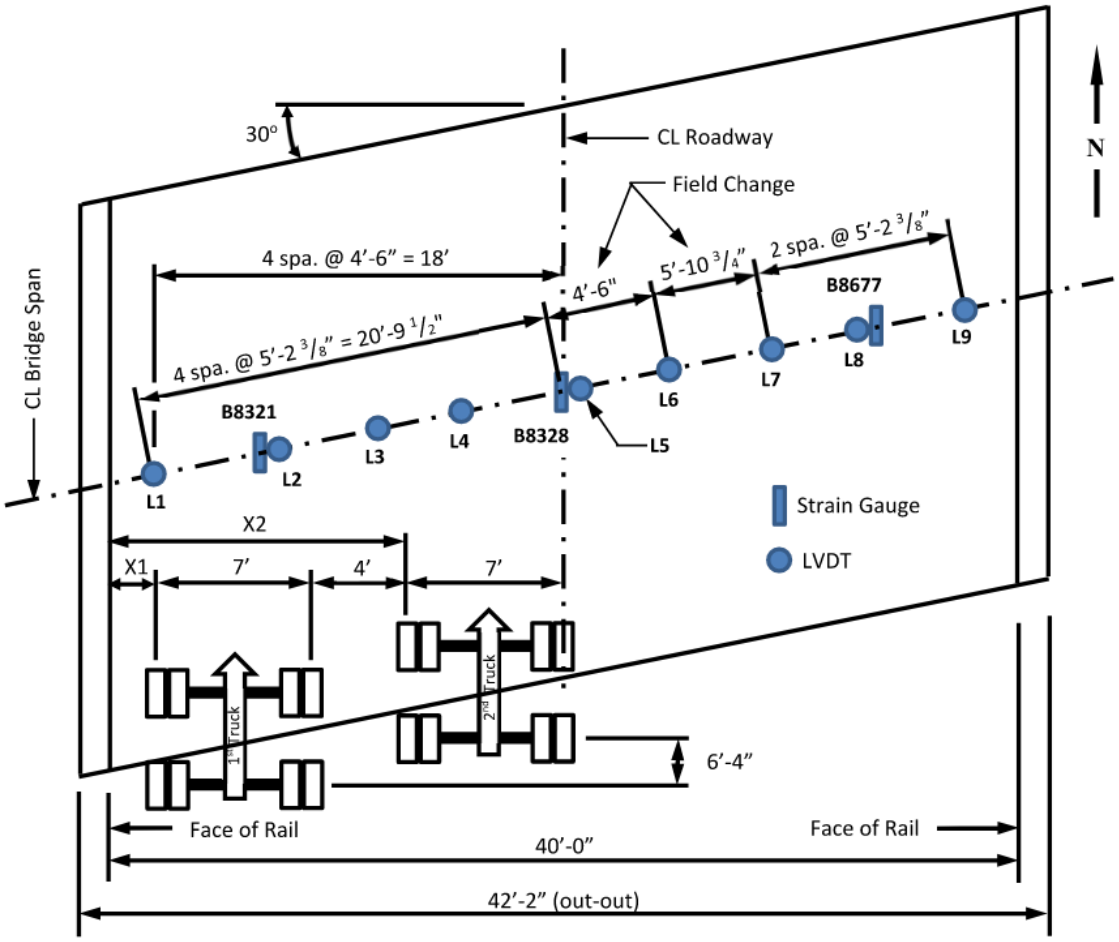

Figure 65. Illustration. Instrumentation plan of 0740016 bridge.

Figure 66. Photo. Photo of instruments under 0740016 bridge.

The target loads for each stage for one truck and two trucks are presented in Table 16 and Table 17, respectively. In the interest of time, it was decided that single-truck loading was not needed, so only two-truck loading was conducted. For incremental loading on the bridge, concrete blocks were added to the trucks. Two different weights can be seen in Figure 67. The bridge was able to carry 100% of the target load without issue. IDOT completed the analysis and results internally.

Table 16. Loading Stages for a Single Truck for 0740016 Bridge

Stage	%	Weight Per Axle (kip)
1	25%	9.9
2	50%	19.9
3	65%	25.9
4	80%	31.8
5	90%	35.8
6	100%	39.8

Table 17. Loading Stages for Two Trucks for 0740016 Bridge

Stage	%	Weight Per Axle (kip)
1	25%	8.6
2	50%	17.3
3	65%	22.5
4	80%	27.7
5	90%	31.1
6	100%	34.6

A. First stage

B. Final stage

Figure 67. Photo. Photographs of testing at different stages of 0740016 bridge.

REFERENCES

American Association of State Highway and Transportation Officials (AASHTO). (2020). *Load and resistance factor design (LRFD) bridge design specifications*. AASHTO.

American Association of State Highway and Transportation Officials & Subcommittee on Bridges and Structures. (2018). *The manual for bridge evaluation*. AASHTO.

American Association of State Highway and Transportation Officials. (2002). *Standard specifications for highway bridges, 17th Ed*. AASHTO.

Amer, A., Arockiasamy, M., & Shahawy, M. (1999). Load distribution of existing solid slab bridges based on field tests. *Journal of Bridge Engineering*, *4*(3), 189–193.

Arockiasamy, M., & Amer, A. (1997). *Load distribution on highway bridges based on field data: Phase 2*. HPR Study0668. Florida Department of Transportation.

Azizinamini, A., Boothby, T. E., Shekar, Y., & Barnhill, G. (1994). Old concrete slab bridges. I: Experimental investigation. *Journal of Structural Engineering*, *120*(11), 3284–3304. https://doi.org/10.1061/(ASCE)0733-9445(1994)120:11(3284)

Bridge Diagnostics, Inc. (n.d.). T500 electrolytic tiltmeter. Retrieved August 21, 2023, from: https://bditest.com/product/t500-electrolytic-tiltmeter/

Colombani, I. A., & Andrawes B. (2022). Comparison of load rating of reinforced concrete slab bridge using analytical and field testing approaches. *Innovative Infrastructure Solutions*, *7*(79), 1–12. https://doi.org/10.1007/s41062-021-00677-9

Commander, B. (2019). Evolution of bridge diagnostic load testing in the USA. *Frontiers in Built Environment*, *5*, 57. https://doi.org/10.3389/fbuil.2019.00057

Davids, W. G., Poulin, T. J., & Goslin, K. (2013). Finite-element analysis and load rating of flat slab concrete bridges. *Journal of Bridge Engineering*, *18*(10), 946–956. https://doi.org/10.1061/(ASCE)BE.1943-5592.0000461

Federal Highway Administration. (2022). ASCE's 2022 Infrastructure Report Card: Bridges. 18-25. https://infrastructurereportcard.org/cat-item/bridges/

Freeman, C. & Vasconcelos, B. (2018). *Solid concrete slab bridges: Effective width recommendations*. Florida Department of Transportation.

Garnica, G. I., Lantsoght, E.O., & Yang. Y. (2022). Monitoring structural responses during load testing of reinforced concrete bridges: A review. *Structure and Infrastructure Engineering*, *18*(10–11): 1558–1580. https://doi.org/10.1080/15732479.2022.2063906

Illinois Department of Transportation. (2017). *Structural service manual*. IDOT.

Jáuregui, D. V., Licon-Lozano, A., & Kulkarni, K. (2010). Higher level evaluation of a reinforced concrete slab bridge. *Journal of Bridge Engineering*, *15*(2), 172–182. https://doi.org/10.1061/(ASCE)BE.1943-5592.0000047

Jones, B.P. (2011). Reevaluation of the AASHTO effective width equation in concrete slab bridge in

Delaware (Master's Thesis, University of Delaware).

Jorgenson, J. L., & Larson, W. (1976). Field Testing of a Reinforced Concrete Highway Bridge to Collapse. 66–71.

Lantsoght, E.O., Van Der Veen C., De Boer A., & Walraven, J. C. (2015) Transverse load redistribution and effective shear width in reinforced concrete slabs. *Heron*, *60*(3), 145–179. http://heronjournal.nl/60-3/2.pdf

Mabsout, M., Tarhini, K., Jabakhanji, R., & Awwad, E. (2004). Wheel load distribution in simply supported concrete slab bridges. *Journal of Bridge Engineering*, *9*(2), 147–155.

Menassa, C., Mabsout, M., Tarhini, K., & Frederick, G. (2007). Influence of skew angle on reinforced concrete slab bridges. *Journal of Bridge Engineering*, *12*(2), 205–214. https://doi.org/10.1061/(ASCE)1084-0702(2007)12:2(205)

Miller R. A., Aktan A. E., & Shahrooz B. M. (1994). Destructive testing of decommissioned concrete slab bridge. *Journal of Structural Engineering*, *120*(7), 2176–2198. https://doi.org/10.1061/(ASCE)0733-9445(1994)120:7(2176)

Saraf, V. K. (1998). Evaluation of existing RC slab bridges. *Journal of Performance of Constructed Facilities*, *12*(1), 20–24. https://doi.org/10.1061/(ASCE)0887-3828(1998)12:1(20)

Shenton III, H. W., & Jones, B. P. (2012). *Effective width of concrete slab bridges in Delaware*. Delaware Department of Transportation.

U.S. Department of Transportation/Federal Highway Administration. (2016). Archived: *Deficient Bridges by Superstructure Type 2016*. https://www.fhwa.dot.gov/bridge/nbi/no10/deck16.cfm.

U.S. Department of Transportation/Federal Highway Administration. (2022). ASCE's 2022 Infrastructure Report Card: Bridges. 18-25. https://infrastructurereportcard.org/cat-item/bridges/

Xu, Y., Brownjohn, J. M. W., & Huseynov F. (2019). Accurate deformation monitoring on bridge structures using a cost-effective sensing system combined with a camera and accelerometers: Case study. *Journal of Bridge Engineering*, *24*(1), 05018014. https://doi.org/10.1061/(ASCE)BE.1943-5592.0001330

Xu, L (2001) Second-order analysis for semi-rigid steel frame design. *Canadian Journal of Civil Engineering* 28: 59–76. https://doi.org/10.1139/l00-077

Zhang, S., & Xu, L. (2017). Bending of rectangular orthotropic thin plates with rotationally restrained edges: A finite integral transform solution. *Applied Mathematical Modelling*, *46*, 48–62. https://doi.org/10.1016/j.apm.2017.01.053


Illinois Department
of Transportation


ILLINOIS